6 Texture zeros in lepton mass matrices of minimal left-right symmetric model

In this chapter, we consider the possibility of texture zeros in the lepton mass matrices of the minimal left-right symmetric model (LRSM) where light neutrino mass arises from a combination of both type I and type II seesaw mechanisms. Based on the allowed texture zeros in light neutrino mass matrix from neutrino and cosmology data, we make a list of all the possible allowed and disallowed texture zeros in Dirac and heavy neutrino mass matrices which appear in type I and type II seesaw terms of LRSM. For the analysis we consider only the cases with maximum possible texture zeros in the light neutrino mass matrix M_ν, Dirac neutrino mass matrix M_D and the heavy neutrino mass matrix M_{RR} while keeping the determinant of M_{RR} non-vanishing, in order to use the standard type I seesaw formula. The possibility of maximum zeros reduces the free parameters of the model making it more predictive. We then compute the new physics contributions to rare decay processes like neutrinoless double beta decay, charged lepton flavor violation. We find that even for a conservative lower limit on the left-right symmetry scale corresponding to heavy charged gauge boson mass 4.5 TeV, in agreement with collider bounds, for right-handed (RH) neutrino masses above 1 GeV, the new physics contributions to these rare decay processes can saturate the corresponding experimental bound.

6.1 Introduction

From the latest global fit of neutrino oscillation data, we see that a few details of the light neutrinos are yet to be determined experimentally. They are namely, the Dirac CP phase, octant of atmospheric mixing angle and the ordering of light neutrinos: normal ordering (NO) or inverted ordering (IO). Also, the nature of neutrinos (Dirac or Majorana) remains unknown at oscillation experiments. If neutrinos are Majorana fermions, there arise two more CP phases known as Majorana CP phases, which can not be determined by oscillation experiments and have to be probed at alternative experiments. Apart from neutrino oscillation experiments, the neutrino sector is constrained by the data from cosmology as well. For example, the latest data from the Planck mission constrain the sum of absolute neutrino masses $\sum_i |m_i| < 0.12$ eV [1]. Although we have significant experimental observations related to the neutrino sector except for the above-mentioned unknowns, the dynamical origin of light neutrino masses and their mixing is still a mystery. The Standard Model (SM) of particle physics, which gives a successful description of all fundamental particles and their interactions (except gravity) can not explain the lightness of neutrinos. The Higgs field in the SM which is responsible for generating masses to all known particles do not have coupling to neutrinos as the RH neutrinos are absent. Several beyond Standard Model (BSM) proposals have been put forward which can explain the tiny neutrino mass. Simplest of which are the seesaw models where a seesaw between the electroweak scale and the scale of newly introduced fields decide the smallness of neutrino masses. As discussed in the earlier chapters, the left-right symmetric model (LRSM) [2, 3, 4, 5, 6, 7, 8, 9, 10, 11, 12] is one of the very popular BSM scenario where the gauge symmetry of the SM is extended to $\mathrm{SU(3)_c \times SU(2)_L \times SU(2)_R \times U(1)_{B-L}}$ so that the RH fermions (which are singlet in SM) can form doublets under the new $SU(2)_R$. This not only makes the inclusion of RH neutrino automatic but also puts the left and RH fermions on equal footing. As we know that in the minimal LRSM, the light neutrino masses arise naturally from a combination of type I and type II seesaw. It should be noted that the idea of combining type I and type II seesaw mechanisms for light neutrino masses was pursued in several earlier works too, for example, [13, 14, 15]. The gauge symmetry, as well as the particle content of minimal LRSM, can also be accommodated within popular grand unified theory (GUT) models like

$SO(10)$. Apart from this, another interesting motivation for this model is its verifiability. A TeV scale LRSM can have very interesting signatures which are being looked at colliders [16, 17, 18]. There also exist different other phenomenological consequences which can be probed at experiments in both the energy as well as intensity frontiers.

Typical seesaw models in the absence of specific flavor symmetries usually predict a very general structure of light neutrino mass matrix which can always be fitted to the observed data due to the presence of many free parameters. The same is true in LRSM as well. However, if the theory has a well-motivated underlying symmetry that gives rise to a very specific structure of the neutrino mass matrix, the number of free parameters can be significantly reduced. In such a case, we can have very specific predictions for light neutrino parameters like CP phase, octant of atmospheric mixing angle, mass ordering which can be tested at ongoing experiments. Here we consider such a possibility where an underlying symmetry can restrict the mass matrix to have non-zero entries only at certain specific locations. Such scenarios are more popularly known as zero texture models, a nice summary of which within three neutrino framework can be found in the review article [19]. Also see [20, 21, 22, 23, 24] for texture related works in different contexts. In the diagonal charged lepton basis, if the light neutrino mass matrix has some textures, the corresponding constraints can be solved to find the light neutrino parameter space that satisfies them. Depending on the viability of this parameter space in view of the latest neutrino oscillation data, one can discriminate between different textures. Also, the allowed textures often predict non-trivial values for unknown parameters that can be tested at different experiments. It has already been shown in earlier works and discussed in the previous chapter that in the diagonal charged lepton basis, not more than two zeros are allowed in the light neutrino mass matrix. While all six possible one zero texture (${}^6C_n, n = 1$) are allowed, among the fifteen possible two zero textures, only six were found to be allowed after incorporating both neutrinos as well as cosmology data [25, 26, 27, 28, 29]. Since in LRSM, several mass matrices play a role in generating light neutrino mass matrix due to the combination of type I and type II seesaw, the requirement of getting the allowed texture zeros in light neutrino mass matrix can constrain the texture zeros of all other mass matrices in the lepton sector namely, the Dirac neutrino mass M_D and heavy neutrino mass M_{RR}. Making a list of all these possibilities while classifying the allowed and disallowed ones is the primary goal of this work. Please

see [30, 31, 32] and references therein for texture zero works in $3+1$ neutrino scenarios and [33] for related phenomenological study of texture zeros in all relevant lepton mass matrices of a particular seesaw model. We not only make such a list considering all possibilities of texture zeros but also perform a numerical analysis for one zero and two zero light neutrino textures as well as a scenario where other mass matrices involved in the seesaw can have a maximum number of zeros. To be more specific, for our numerical analysis, we considered five zero textures in M_D and four zero textures in M_{RR}, keeping the rank of the latter three. Out of 378 total possibilities belonging to this list, we find that 189 are allowed from light neutrino data, out of which 109 give rise to two zero textures in light neutrino mass matrix. The case for a maximum number of zeros is particularly chosen due to their more predictive nature. We not only find the correlations among light neutrino parameters but also find all the new physics contribution to other interesting processes like neutrinoless double beta decay (NDBD) and charged lepton flavor violation (CLFV) that arises in the LRSM scenario. As these processes are being probed at several experiments, this study points out the possibility of probing such scenarios at those experiments. Such aspects of probing LRSM can be complementary to the ongoing collider searches mentioned earlier.

This chapter is organised as follows. In section 6.2, we discuss in details the texture structures of the Dirac and Majorana mass matrices in LRSM. We then summarise the contributions to NDBD and CLFV in LRSM in section 6.3, 6.4 respectively. We discuss our numerical analysis and results in section 6.5 and then finally conclude in section 6.6.

6.2 Texture Zeros in Lepton Mass Matrices of LRSM

As has been mentioned in the earlier chapters, the left-right symmetric model is a very well motivated and widely studied extension of the SM with an enlarged gauge symmetry based on $\mathrm{SU(3)_c \times SU(2)_L \times SU(2)_R \times U(1)_{B-L}}$ [2, 3, 4, 5, 6, 7, 8, 9, 10, 11, 12]. The theory removes the disparity between the left and RH fields by considering the RH fields to be doublet under the additional $SU(2)_R$ keeping the right sector couplings same as the left one by left-right symmetry. The light neutrino mass after symmetry breaking is generated within a type I+II seesaw as defined in equation (5.5),

Without any loss of generality, we make use of rotation in the $SU(2)_L \times SU(2)_R$ space so that only one of the neutral components of the Higgs bidoublet acquires a large vacuum expectation value, $k_1 \approx v_{\rm SM}$ and $k_2 \approx 0$. This corresponds to negligible mixing ξ. Under these assumptions, the Dirac neutrino mass matrix and the charged lepton mass matrix are given by,

$$M_D = \frac{1}{\sqrt{2}}(k_1 h), M_l = \frac{1}{\sqrt{2}}(k_1 \tilde{h}), \tag{6.1}$$

which points out the freedom in choosing M_l and M_D as we do in the subsequent sections.

As mentioned earlier, texture zeros in lepton mass matrices increase the predictive power of the model due to a decrease in the number of free parameters [19, 20, 21, 22, 25, 26, 27, 28, 29]. Since the light neutrino mass comes from a combination of type I seesaw term $M_D {M_{RR}}^{-1} {M_D}^T$ and a type II seesaw term $M_{LL} \propto M_{RR}$, the requirement of having allowed number of zeros in the light neutrino mass matrix can constrain the texture zeros in M_D, M_{RR} in an interesting way. Although M_ν can have at most six zeros (only 6 out of 15 allowed), we can have more texture zero possibilities in M_D, M_{RR}. Since M_D is not necessarily Hermitian, we can have nine independent elements so that n texture zeros can have ${}^9C_n$ possibilities. On the other hand, M_{RR}, being complex symmetric can have six independent elements will have ${}^6C_n$ possibilities for n texture zeros. While finding texture zeros in M_{RR} we, however, make sure that the determinant is non-zero so that the type I seesaw formula can be applied. We classify these texture zero possibilities as follows.

- The different classes of 4-0 texture $\rm M_{RR}$ with non-zero determinant are:

$$\rm M_{RR} = \begin{bmatrix} 0 & w & 0 \\ w & 0 & 0 \\ 0 & 0 & x \end{bmatrix}, M_{RR} = \begin{bmatrix} 0 & 0 & w \\ 0 & x & 0 \\ w & 0 & 0 \end{bmatrix}, M_{RR} = \begin{bmatrix} w & 0 & 0 \\ 0 & 0 & x \\ 0 & x & 0 \end{bmatrix} \tag{6.2}$$

- The different classes of 3-0 texture $\rm M_{RR}$ with non-zero determinant are:

$$\rm M_{RR} = \begin{bmatrix} 0 & 0 & w \\ 0 & x & y \\ w & y & 0 \end{bmatrix}, M_{RR} = \begin{bmatrix} 0 & w & x \\ w & 0 & y \\ x & y & 0 \end{bmatrix}, M_{RR} = \begin{bmatrix} 0 & w & 0 \\ w & x & 0 \\ 0 & 0 & y \end{bmatrix} \tag{6.3}$$

$$\rm M_{RR} = \begin{bmatrix} 0 & 0 & w \\ 0 & x & 0 \\ w & 0 & y \end{bmatrix}, M_{RR} = \begin{bmatrix} 0 & w & 0 \\ w & 0 & x \\ 0 & x & y \end{bmatrix}, M_{RR} = \begin{bmatrix} w & 0 & 0 \\ 0 & 0 & x \\ 0 & x & y \end{bmatrix} \tag{6.4}$$

$$\mathrm{M_{RR}} = \begin{bmatrix} w & 0 & 0 \\ 0 & x & y \\ 0 & y & 0 \end{bmatrix}, \mathrm{M_{RR}} = \begin{bmatrix} w & 0 & 0 \\ 0 & x & 0 \\ 0 & 0 & y \end{bmatrix}, \mathrm{M_{RR}} = \begin{bmatrix} w & x & 0 \\ x & 0 & 0 \\ 0 & 0 & z \end{bmatrix} \tag{6.5}$$

$$\mathrm{M_{RR}} = \begin{bmatrix} w & x & 0 \\ x & 0 & y \\ 0 & y & 0 \end{bmatrix}, \mathrm{M_{RR}} = \begin{bmatrix} 0 & w & 0 \\ w & 0 & x \\ 0 & x & y \end{bmatrix}, \mathrm{M_{RR}} = \begin{bmatrix} 0 & w & 0 \\ w & x & 0 \\ 0 & 0 & y \end{bmatrix} \tag{6.6}$$

$$\mathrm{M_{RR}} = \begin{bmatrix} w & x & 0 \\ x & 0 & y \\ 0 & y & 0 \end{bmatrix} \tag{6.7}$$

- The different classes of 2-0 texture $\mathrm{M_{RR}}$ with non-zero determinant are:

$$M_{RR} = \begin{bmatrix} 0 & 0 & w \\ 0 & x & y \\ w & y & z \end{bmatrix}, \mathrm{M_{RR}} = \begin{bmatrix} 0 & x & 0 \\ x & y & z \\ 0 & z & u \end{bmatrix}, \mathrm{M_{RR}} = \begin{bmatrix} w & x & 0 \\ x & 0 & y \\ 0 & y & z \end{bmatrix} \tag{6.8}$$

$$\mathrm{M_{RR}} = \begin{bmatrix} w & 0 & x \\ 0 & y & z \\ x & z & u \end{bmatrix}, \mathrm{M_{RR}} = \begin{bmatrix} w & 0 & x \\ 0 & 0 & y \\ x & y & z \end{bmatrix}, \mathrm{M_{RR}} = \begin{bmatrix} w & x & 0 \\ x & y & z \\ 0 & z & u \end{bmatrix} \tag{6.9}$$

$$\mathrm{M_{RR}} = \begin{bmatrix} w & x & y \\ x & 0 & z \\ y & z & 0 \end{bmatrix}, \mathrm{M_{RR}} = \begin{bmatrix} w & x & y \\ x & 0 & 0 \\ 0 & 0 & z \end{bmatrix}, \mathrm{M_{RR}} = \begin{bmatrix} w & x & y \\ x & z & 0 \\ y & 0 & 0 \end{bmatrix} \tag{6.10}$$

$$\mathrm{M_{RR}} = \begin{bmatrix} 0 & w & x \\ w & 0 & y \\ x & y & z \end{bmatrix}, \mathrm{M_{RR}} = \begin{bmatrix} 0 & w & x \\ w & y & z \\ x & z & 0 \end{bmatrix}, \mathrm{M_{RR}} = \begin{bmatrix} 0 & w & x \\ w & y & 0 \\ x & 0 & z \end{bmatrix} \tag{6.11}$$

$$\mathrm{M_{RR}} = \begin{bmatrix} w & 0 & 0 \\ 0 & x & y \\ 0 & y & z \end{bmatrix}, \mathrm{M_{RR}} = \begin{bmatrix} w & 0 & x \\ 0 & y & 0 \\ x & 0 & z \end{bmatrix}, \mathrm{M_{RR}} = \begin{bmatrix} w & x & 0 \\ x & y & 0 \\ 0 & 0 & z \end{bmatrix} \tag{6.12}$$

- The different classes of 1-0 texture $\mathrm{M_{RR}}$ with non-zero determinant are:

$$\mathrm{M_{RR}} = \begin{bmatrix} 0 & w & x \\ w & y & z \\ x & z & u \end{bmatrix}, \mathrm{M_{RR}} = \begin{bmatrix} w & 0 & x \\ 0 & y & z \\ x & z & u \end{bmatrix}, \mathrm{M_{RR}} = \begin{bmatrix} w & x & 0 \\ x & 0 & y \\ 0 & y & z \end{bmatrix} \tag{6.13}$$

$$\mathrm{M_{RR}} = \begin{bmatrix} w & x & y \\ x & 0 & z \\ y & z & u \end{bmatrix}, \mathrm{M_{RR}} = \begin{bmatrix} w & x & y \\ x & z & 0 \\ y & 0 & u \end{bmatrix}, \mathrm{M_{RR}} = \begin{bmatrix} w & x & y \\ x & z & u \\ y & u & 0 \end{bmatrix} \tag{6.14}$$

The different number of allowed texture structures obtained for the various combinations of 5-0, 4-0, 3-0, 2-0 and 1-0 M_D with 4-0, 3-0, 2-0, 1-0 M_{RR} are shown in tabular form in table 6.1. However, for detailed numerical analysis, we will consider the RH Majorana mass matrix with the highest number of zeros, i.e., 4-0 texture M_{RR} as given by equation (6.2). Similarly, we will consider M_D with 5 zeros (maximum) which can phenomenologically provide the allowed zero textures in the light neutrino mass matrix.

M_D/M_{RR} textures	Total textures	1-0(A)	2-0(A)	No-0(A)	Total (A)
5-0 / 4-0	378	62	109	18	189
5-0 / 3-0	1638	628	23	481	1132
5-0 / 2-0	1890	553	73	1155	1781
4-0 / 4-0	378	161	76	70	307
4-0 / 3-0	1638	504	114	928	1546
4-0 / 2-0	1890	277	34	1534	1845
4-0 / 1-0	756	40		716	756
3-0 / 4-0	252	78		133	211
3-0 / 3-0	1092	168	19	896	1083
3-0 / 2-0	1260	68	6	1179	1253
3-0 / 1-0	504	9		495	504
2-0 / 4-0	108	12		96	108
2-0 / 3-0	468	15		453	468
2-0 / 2-0	540	4		536	540
2-0 / 1-0				216	216
1-0 / 4-0	27			27	27
1-0 / 3-0	117			117	117
1-0 / 2-0	135			135	135
1-0 / 1-0	54			54	54

Table 6.1: Different number of allowed (A) texture zero neutrino mass for different textures of M_D and M_{RR}. The blank boxes mean no possibilities.

M_{RR}	1-0(A)	2-0(A)	No-0(A)	2-0(NA)	3-0(NA)	4-0(NA)	Total M_D
1	20	27	6	48	23	2	126
2	20	27	6	51	20	2	126
3	22	55	6	21	20	2	126

Table 6.2: Number of different textures obtained for 5-0 M_D, 4-0 M_{RR} (with rank 3). A and NA in brackets represent allowed and not allowed cases.

Furthermore, from table 6.2, we will take into consideration only the allowed cases of two texture zero structures of light neutrino mass matrix. Out of a total of ${}^6C_2$ i.e., 15 two texture zeros of ν mass matrix, 6 are totally allowed by neutrino and cosmology data. It should be noted that these conclusions hold for diagonal charged lepton basis which we also adopt in our analysis. Since we have only three possible M_{RR} structures with non-zero determinants (as given in equations 6.2), the possibilities of obtaining the allowed two zero texture neutrino mass matrix for a particular texture of M_{RR} are also limited. The allowed two zero textures obtained for the three different M_{RR} textures are (A2, B1), (A1, B2) and (B1, B2, B3, B4) respectively for M_D with five zeros. Herein we have picked up these combinations of M_D and M_{RR} which lead to the allowed class of two zero texture neutrino mass in the framework of minimal LRSM.

- **For the class A1** ($M_{ee} = 0, M_{e\mu} = 0$)

$$\mathrm{M_{RR}} = \begin{bmatrix} 0 & 0 & w \\ 0 & x & 0 \\ w & 0 & 0 \end{bmatrix}, \mathrm{M_D} = \begin{bmatrix} 0 & 0 & a_3 \\ 0 & b_2 & 0 \\ 0 & c_2 & c_3 \end{bmatrix} \tag{6.15}$$

- **For the class A2** ($M_{ee} = 0, M_{e\tau} = 0$)

$$\mathrm{M_{RR}} = \begin{bmatrix} 0 & w & 0 \\ w & 0 & 0 \\ 0 & 0 & x \end{bmatrix}, \mathrm{M_D} = \begin{bmatrix} 0 & 0 & 0 \\ 0 & b_3 & 0 \\ c_1 & c_2 & c_3 \end{bmatrix} \tag{6.16}$$

- **For the class B1** ($M_{e\tau} = 0, M_{\mu\mu} = 0$)

$$\mathrm{M_{RR}} = \begin{bmatrix} w & 0 & 0 \\ 0 & 0 & x \\ 0 & x & 0 \end{bmatrix}, \mathrm{M_D} = \begin{bmatrix} 0 & a_2 & a_3 \\ 0 & b_2 & 0 \\ c1 & 0 & 0 \end{bmatrix} \tag{6.17}$$

$$\mathrm{M_{RR}} = \begin{bmatrix} 0 & w & 0 \\ w & 0 & 0 \\ 0 & 0 & x \end{bmatrix}, \mathrm{M_D} = \begin{bmatrix} a_1 & 0 & a_3 \\ 0 & b_2 & 0 \\ c_1 & 0 & 0 \end{bmatrix} \tag{6.18}$$

- **For the class B2** ($M_{e\mu} = 0, M_{\tau\tau} = 0$)

$$\mathrm{M_{RR}} = \begin{bmatrix} w & 0 & 0 \\ 0 & 0 & x \\ 0 & x & 0 \end{bmatrix}, \mathrm{M_D} = \begin{bmatrix} 0 & 0 & a_3 \\ b_1 & 0 & b_3 \\ 0 & c_2 & 0 \end{bmatrix} \tag{6.19}$$

$$\mathrm{M_{RR}} = \begin{bmatrix} 0 & 0 & w \\ 0 & x & 0 \\ w & 0 & 0 \end{bmatrix}, \mathrm{M_D} = \begin{bmatrix} a_1 & a_2 & 0 \\ b_1 & 0 & 0 \\ 0 & 0 & c_3 \end{bmatrix} \tag{6.20}$$

- **For the class B3** ($M_{e\mu} = 0, M_{\mu\mu} = 0$)

$$\mathrm{M_{RR}} = \begin{bmatrix} w & 0 & 0 \\ 0 & 0 & x \\ 0 & x & 0 \end{bmatrix}, \mathrm{M_D} = \begin{bmatrix} 0 & a_2 & a_3 \\ 0 & 0 & 0 \\ c_1 & 0 & c_3 \end{bmatrix} \tag{6.21}$$

- **For the class B4** ($M_{\mu\mu} = 0, M_{\tau\tau} = 0$)

$$\mathrm{M_{RR}} = \begin{bmatrix} w & 0 & 0 \\ 0 & 0 & x \\ 0 & x & 0 \end{bmatrix}, \mathrm{M_D} = \begin{bmatrix} 0 & a_2 & 0 \\ b_1 & b_2 & b_3 \\ 0 & 0 & 0 \end{bmatrix} \tag{6.22}$$

Although our study is motivated from a phenomenological point of view, it is worth mentioning that the texture zeros in fermion mass matrices can have dynamical origin from flavor symmetries. See, for example, the scenarios proposed in [34, 35, 36, 37, 38, 39, 40, 41, 42] where discrete as well as continuous symmetries were considered to explain the texture zeros.

In particular, the recent work [36] considered a different version of LRSM where charged fermions receive masses from a universal seesaw mechanism while neutrinos acquire masses at the radiative level. A non-abelian discrete flavor symmetry based on the $\triangle(27)$ group was incorporated, leading to predictive textures of different fermion mass matrices. We leave such a flavor symmetric explanation of the textures considered here for future works.

Phenomenological implications of two texture zero M_ν on low energy phenomena like NDBD and CLFV have been analyzed in the previous chapter. However, in that case, the authors have considered the two zero texture mass matrix to be favouring a tri-maximal mixing pattern. Besides, all the contributions to NDBD that could arise in the framework of LRSM were not taken into consideration. Here we generalize this to consider maximum allowed texture zeros that is 5-0 M_D and 4-0 M_{RR} giving rise to the allowed two zero texture neutrino mass matrix and then study the implications of these M_D and M_{RR} for NDBD, considering all the possible contributions that could arise in LRSM and also study for lepton flavor violating processes like $\mu \to e\gamma$ and $\mu \to 3e$.

6.3 Neutrinoless Double Beta Decay in LRSM

For a review and recent status of neutrinoless double beta decay, please refer to [43, 44, 45]. Apart from probing the intrinsic nature of light neutrinos, NDBD can also be used to discriminate between neutrino mass hierarchies: normal versus inverted. From the measurement of NDBD half-life combined with sufficient information about the phase space factors (PSF) and associated nuclear matrix element (NME), one can set constraints on the absolute neutrino mass scales. If light neutrinos are Majorana, we can get a sizable contribution to NDBD especially when the ordering is of inverted type. There have been several works where BSM contributions to NDBD have been calculated. For example, see [46, 47, 48, 49, 50, 51] and references therein. In the LRSM scenario, it has been widely studied in several earlier works including [52, 53, 54, 55, 56, 57, 58, 59, 60, 61, 62, 63]. Due to the presence of many new heavy particles in LRSM, sizable new contributions of NDBD decay amplitudes arises which may be dominant over the standard mechanism mediated by light neutrinos some of which has been dicussed in the earlier chapters. Out of the different NDBD experiments, KamLAND-Zen [64] has reported a strong lower limit on the half-life

from searches on $^{1}36Xe$ as $T^{0\nu}_{1/2} > 1.07 \times 10^{26}$ year at 90% C. L. This can be translated to an upper limit of effective Majorana mass in the range $(0.061 - 0.165)$ eV where the uncertainty arises due to the NME.

We show all the contributions to NDBD in minimal LRSM in terms of corresponding Feynman diagrams in figure 1.4, 1.5, 1.6, 1.7 in chapter 1. We now list their respective contributions below one by one following the notations of [63].

- When light and heavy neutrinos are the source of NDBD mediated by purely left handed (LH) currents ($W_L - W_L$) as shown in figure 1.4 in chapter 1, the corresponding amplitudes are given by,

$$A_\nu{}^{LL} \propto G_F^2 \sum_i \frac{U_{e_i}{}^2 m_i}{p^2}, A_N{}^{LL} \propto G_F^2 \sum_i \frac{S_{e_i}{}^2 M_i}{p^2}. \tag{6.23}$$

  where, $|p| \sim 100$ MeV is the typical momentum transfer at the leptonic vertex, U and S represent the mixing matrices as given in equations (1.82) and (1.84), m_i and M_i are the masses for the three generations of light and heavy Majorana neutrinos respectively.

- The RH current mediated by W_R can contribute to NDBD through the exchange of the light as well as heavy neutrino N (as shown in figure 1.5). The corresponding amplitudes are given by,

$$A_\nu{}^{RR} \propto G_F^2 \sum_i \left(\frac{M_{W_L}}{M_{W_R}}\right)^4 \left(\frac{g_R}{g_L}\right)^4 \frac{T^*_{e_i}{}^2 m_i}{p^2}, \tag{6.24}$$

$$A_N{}^{RR} \propto G_F^2 \sum_i \left(\frac{M_{W_L}}{M_{W_R}}\right)^4 \left(\frac{g_R}{g_L}\right)^4 \frac{V^*_{e_i}{}^2 M_i}{p^2}, \tag{6.25}$$

  where, M_{W_L} and M_{W_R} are the mass of the LH and RH gauge bosons respectively.

- Significant Contribution can also arise due to the mixed helicity diagrams, mediated by both W_L and W_R (λ contribution) and from diagrams mediated by $W_L - W_R$ mixing (η contribution), the amplitudes of which are given as,

$$A_\lambda \propto G_F^2 \sum_i \left(\frac{M_{W_L}}{M_{W_R}}\right)^2 \frac{U_{e_i} T^*_{e_i}}{p}, A_\eta \propto G_F^2 \sum_i \tan\xi \frac{U_{e_i} T^*_{e_i}}{p}, \tag{6.26}$$

  where ξ is the L-R gauge boson mixing parameter as described earlier.

- Further, there is also the scalar triplet ($\Delta_{L,R}$) contributions to NDBD by the mediations of W_L and W_R gauge bosons respectively, the amplitude of which depends upon the masses of these gauge bosons and given by,

$$\mathrm{A_{\Delta_L}} \propto \mathrm{G_F^2} \frac{\left(\mathrm{M_\nu}^{\mathrm{II}}\right)_{\mathrm{ee}}}{\mathrm{M_{\Delta_L}^{++2}}}, \mathrm{A_{\Delta_R}} \propto \mathrm{G_F^2} \left(\frac{\mathrm{M_{W_L}}}{\mathrm{M_{W_R}}}\right)^4 \frac{\mathrm{V_{e_i}}^2 \mathrm{M_i}}{\mathrm{M_{\Delta_R}^{++2}}} \tag{6.27}$$

  where the contribution from left triplet scalar is negligible due to smallness of v_L as well as the smallness of light neutrino mass contribution coming from type II seesaw.

The particle physics parameters governing NDBD for the different contributions (ignoring the left triplet Higgs contribution) in LRSM we have considered are given by,

$$|\eta_\nu| = \frac{1}{m_e} \sum_i U_{e_i}^2 m_i \tag{6.28}$$

$$\left|\eta_{N_R}^L\right| = m_p \sum_i \frac{S_{e_i}^2}{m_i} \tag{6.29}$$

$$\left|\eta_{N_R+\Delta_R}^R\right| = m_p \left(\frac{M_{W_L}}{M_{W_R}}\right)^4 \left(\sum_i \frac{V_{e_i}^2}{M_i} + \sum_i \frac{V_{e_i}^2 M_i}{{M_{\Delta_R}}^2}\right) \tag{6.30}$$

$$|\eta_\lambda| = \left(\frac{M_{W_L}}{M_{W_R}}\right) \left|\sum_i U_{e_i} T_{e_i}^*\right|. \tag{6.31}$$

$$|\eta_\eta| = \tan\xi \left|\sum_i U_{ei} T_{ei}^*\right|. \tag{6.32}$$

In the above equations, m_p and m_e are the mass of the proton and electron respectively. It is seen that the amplitudes of these processes are mostly dependent on the mixing between neutrinos, the mass of the heavy neutrinos, $\mathrm{N_i}$, the mass of the gauge bosons, $\mathrm{{W_L}^-}$ and $\mathrm{{W_R}^-}$, mass of doubly charged scalars triplet Higgs, Δ_L and Δ_R as well as their coupling to leptons, $\mathrm{f_L}$ and f_R. The total analytic expression for the inverse half-life governing NDBD considering all the dominant contributions that could arise in LRSM is given by,

$$\left[T_{\frac{1}{2}}^{0\nu}\right]^{-1} = G^{0\nu}(Q,Z) \left(\left|M_\nu^{0\nu}\eta_\nu + M_N^{0\nu}\eta_{N_R}^L\right|^2 + \left|M_N^{0\nu}\eta_{N_R}^R + M_N^{0\nu}\eta_{\Delta_R}\right|^2 + \left|M_\lambda^{0\nu}\eta_\lambda + M_\eta^{0\nu}\eta_\eta\right|^2\right), \tag{6.33}$$

In the above expression, $G^{0\nu}(Q,Z)$ represents the phase space factor and $M^{0\nu}$ is the nuclear matrix element which have different values for different contributions which is shown in tabular form in table 6.3 [62].

Isotope	$G^{0\nu}(Q,Z)(yr^{-1})$	$M_\nu^{0\nu}$	$M_N^{0\nu}$	$M_\lambda^{0\nu}$	$M_\eta^{0\nu}$
76_{Ge}	5.77×10^{-15}	2.58-6.64	233-412	1.75-3.76	235-637
136_{Xe}	3.56×10^{-14}	1.57-3.85	164-172	1.92-2.49	370-419

Table 6.3: The different values of PSF and NME for different nuclei used in NDBD experiments.

6.4 Charged Lepton Flavor Violation in LRSM

Charged lepton flavor violation arises in the SM at one-loop level and remains suppressed by the smallness of neutrino masses, much beyond the current and near-future experimental sensitivities. Therefore, any experimental observation of such processes is a sign of BSM physics, like the one we are studying here. For a review of CLFV in SM and beyond, please refer to [65]. Though usual light neutrino contribution to CLFV is negligible, presence of heavy neutrinos in BSM frameworks can give rise to observable CLFV [66, 67, 68, 69, 70, 63, 71, 58, 61, 72]. In LRSM, sizable CLFV occurs dominantly due to the contributions arising from the additional scalars and the heavy neutrinos. Among the various processes that violate lepton flavor, the most relevant ones are the rare leptonic decay modes of the muon, notably, $(\mu \to e\gamma)$ and $(\mu \to 3e)$. The best upper limit for the branching ratio (BR) of these processes are provided by MEG collaboration [73] and SINDRUM experiment [74] which provide the corresponding upper limit as $\mathrm{BR}\,(\mu \to e\gamma) < 4.2 \times 10^{-13}$ and $\mathrm{BR}\,(\mu \to 3e) < 1.0 \times 10^{-12}$ respectively.

6.5 Numerical Analysis and Results

For our numerical analysis, we first parameterize the light neutrino mass matrix in terms of the Pontecorvo-Maki-Nakagawa-Sakata (PMNS) leptonic mixing matrix which is related to the diagonalizing matrices of neutrino and charged lepton mass matrices U_ν, U_l respectively as,

$$U_{\mathrm{PMNS}} = U_l^\dagger U_\nu \tag{6.34}$$

In the diagonal charged lepton basis, considered in this work, we can write the light neutrino mass matrix as,

$$M_\nu = U_{\rm PMNS} {M_\nu}^{(\rm diag)} {U_{\rm PMNS}}^T \tag{6.35}$$

where ${M_\nu}^{(\rm diag)} = \rm diag(m_1, m_2, m_3)$. We first implement the texture zero conditions on the light neutrino mass matrix and numerically solve the texture zero conditions to find the allowed parameter space. As pointed out earlier, there are six one zero texture possibilities whereas out of the fifteen possible two zero textures, only six of them are compatible with neutrino and cosmology data which are labelled here as A1, A2, B1, B2, B3 and B4. Out of the nine parameters of the neutrino mass matrix, five are fixed by experimental measurements of the two mass-squared differences and three mixing angles. The remaining four parameters namely, $m_{\rm lightest} = m_1(\rm NO)/m_3(\rm IO), \delta, \alpha, \beta$ which are not measured yet, can be predicted by the texture zero conditions. This is possible in two zero texture cases particularly, because of two texture zero conditions which give rise to four real equations that can be solved simultaneously to find four unknown parameters. We vary the five known parameters randomly in the 3σ range using the recent global fit [75]. Using the latest data, we found that out of the previously allowed six possible two zero textures, A2 for both NO and IO and A1 (IO) are disallowed. We consider the allowed ones for our analysis for NDBD and CLFV. For representative purpose, we show some correlations between light neutrino parameters coming out from the two zero texture conditions in figure 6.1, 6.2, 6.3. Similar correlation plots were obtained in earlier work [29].

In minimal LRSM, the neutrino mass is given by equation ((5.5)) where the first and second terms represent the type II and type seesaw mass terms respectively. γ is the dimensionless parameter that appears from the minimization of the scalar potential, defined before. We have fine-tuned the dimensionless parameter $\gamma = 10^{-9}$ to obtain the neutrino mass of the order of sub eV. This is chosen particularly to keep the RH neutrino masses in the desired range. The RH neutrino mass matrix, defined earlier, is $M_{RR} = \sqrt{2} v_R f_R = \frac{v_R}{v_L} {M_\nu}^{II} = \frac{v_R^2}{\gamma v_{\rm SM}^2} {M_\nu}^{II}$. The choice of v_R for a few TeV W_R mass, and type II seesaw term at sub-eV scale, the chosen value of γ keeps the RH neutrino mass above 1 GeV. This is required to ensure that for the heavy neutrino mediated processes of NDBD, the masses of mediators remain above the typical momentum exchange of the process ~ 100 MeV. For heavy neutrino masses below this scale, the contribution to NDBD will be different, see for example [76].

Recent ATLAS and CMS data enforce the W_R boson to be heavier than about at least 3 TeV, the exact bound depending on the RH neutrino sector [16, 17, 77]. We consider it to be $M_{W_R} = 4.5$ TeV, which satisfy the latest collider bounds [77] for our chosen values of RH neutrino mass spectrum. All other relevant parameters of minimal LRSM which are used in the calculations are shown in table 6.4. It is worth noting that the chosen doubly charged scalar masses respect the latest bounds from collider experiment. Based on the results of the ATLAS searches for same-sign dileptonic new physics signals [78], there is a lower bound on the masses of the doubly-charged scalars $\Delta_L^{\pm\pm}$ and $\Delta_R^{\pm\pm}$. Assuming that the branching ratios into electronic and muonic final states are both equal to 50%, the $SU(2)_L$ and $SU(2)_R$ doubly-charged Higgs-boson masses have to be larger than 785 GeV and 675 GeV respectively. Our conservative lower bound on charged scalars from these triplets agree with all such experimental data.

Having determined the light neutrino parameters which satisfy the two zero texture conditions, we then numerically determine the elements of M_D, M_{RR} for the chosen textures. We then use the corresponding M_D, M_{RR} as well as the light neutrino mass matrix for computing the relevant contributions to NDBD and CLFV. For NDBD mediated by the light Majorana neutrinos, the half-life of the decay process is given by equation (1.91), Γ represents the decay width for $0\nu\beta\beta$ decay process, m_e is the electron mass and the terms $G^{0\nu}$ and $|M^{0\nu}|$ represents the phase space factor and the nuclear matrix elements respectively which holds different values as shown in table 6.3. The effective light neutrino mass is given by equation (1.92). There are contributions coming from heavy RH neutrinos and right scalar Higgs triplets, both having an exchange of W_R bosons. The effective neutrino mass corresponding to these dominant contributions is given by equation (4.11). We have also considered the momentum dependent contributions to NDBD i.e., the λ and η contributions to NDBD. The particle physics parameter that measures the lepton number violation in case of λ and η contribution, are given by equations (6.31) and (6.32). The effective Majorana neutrino mass due to λ and η contribution is given by equation (3.14).

We evaluated the half-lives for the different contributions to NDBD with respect to the elements in M_D and M_{RR} as well as for the total contribution using equation (6.33), for the classes A1 (NO) and B1, B2, B3, B4 (NO and IO). The half-lives corresponding to the individual contributions in the LRSM framework are shown in figures 6.5 to 6.14 and the

half-life from the total contribution is shown in figure 6.15 to 6.19. Apart from the light neutrino contribution, we show the individual as well as a total contribution to half-life in terms of the parameters in M_D, M_{RR} for the chosen classes discussed in section 6.2. The parameters $a1, a2, a3, b1, b2, b3, c1, c2, c3$ correspond to different entries in different chosen textures of M_D while w, x correspond to non-zero entries in M_{RR}.

Parameter	Value
γ	10^{-9}
ξ	10^{-6}
$M_{\Delta_R{}^{++}} \approx M_{\Delta_L{}^{++}} \approx M_{\Delta_L{}^{+}}$	1 TeV
M_{W_L}	80 GeV
M_{W_R}	4.5 TeV

Table 6.4: The numerical values of different parameters in minimal LRSM adopted in our numerical analysis

From figure 6.1 to 6.3, we have shown the correlation between different neutrino parameters in the framework of LRSM for both normal and inverted hierarchies. Figures 6.5 and 6.6 represent the half-life governing NDBD for different individual contributions in LRSM for the class A1. Furthermore, due to $[M_\nu]_{ee} = 0$, the standard light neutrino contribution does not arise in this case. Again, as seen in equation (6.15), $[M_{RR}]_{ee} = 0$ for the class A1, so the heavy neutrino contributions mediated by RH currents also cease to exist in this case. Due to the inconsistency of IO with experimental data, we have analysed only for the normal case. In figures 6.7 and 6.8, we have shown the half-life for the class B1 for both the mass hierarchies. However, it is seen that the mixed contributions do not arise in this case as the factor governing NDBD for the left-right mixing, $\left[M_D M_{RR}^{-1}\right]_{ee}$ is almost negligible in this case. Similar results hold for the classes B2, B3 and B4. For the classes, B2, B3 and B4 we have shown the individual contributions in figures 6.9 to 6.10, 6.11 to 6.12, 6.13 to 6.14 respectively. We have also shown the total contributions to NDBD in LRSM scenario in the figures 6.15 to 6.19 for the different allowed classes of two zero texture neutrino mass. In all the classes, we have varied the half-life governing NDBD with the parameters in the Dirac and Majorana mass matrix M_D and M_{RR} and compared with the experimental lower limit provided by the KamLAND-Zen experiment [64]. In figure 6.4 we have shown the standard

light neutrino contribution to half-life as a function of the sum of the absolute neutrino masses considering the PLANCK bound $\sum_i |m_i| < 0.12$ eV [1]. From the figures, we can conclude that only NO satisfies the experimental bounds for all the classes, B1-B4. In figure 6.20, we plotted the total contribution to NDBD with the lightest RH neutrino mass to see the parameter space of the heavy RH neutrino mass satisfying NDBD.

Furthermore, we have also evaluated the branching ratio of the CLFV process $\mu \to e\gamma$ with respect to the elements of M_D and M_{RR} for the different classes of two zero texture neutrino mass for both normal and inverted hierarchies. For calculating the BR, we used the expression given in equation (1.107). The relevant calculations were done by diagonalizing the RH neutrino mass matrix and obtaining the mixing matrix element, V_{ij} and the eigenvalues M_i. The results obtained have been summarized in the figures 6.21 to 6.25 where the BR is plotted as a function of parameters in M_D, M_{RR}, along with the comparison with MEG upper bound. Furthermore, we have also studied the BR for the LFV process ($\mu \to 3e$) and show the results in figure 6.26 with the parameters in M_D and M_{RR} for the different classes and compared with the experimental upper bound provided by the SINDRUM experiment. The BR for both the CLFV processes has a strong dependence on the RH neutrino mixing matrix structure. Interestingly, we see that IO occupies very less parameter space within experimental bound in comparison to NO. For the class B4, all the parameter space is ruled out by MEG upper limit. For the process ($\mu \to 3e$), the BR is controlled by $\mathrm{h}'_{\mu e}\mathrm{h}'^{*}_{ee}$ which vanishes for the classes A1, B2, B3 and B4 due to vanishing $\mathrm{h}'_{\mu e}$ because of the structure of M_{RR}. Whereas for the classes B1, using the structures of M_D and M_{RR} as shown in equation (6.18) we arrive at the BR as shown in figure 6.26. Again, we can see from our analysis that the observables for NDBD and CLFV are highly dependent on the Dirac and Majorana mass matrices and their structures which are again different for the different classes of the two zero texture light neutrino mass matrix.

It is worth mentioning that several earlier works [55, 61] found that the NDBD and CLFV limits induce a hierarchy between the mass of the $SU(2)_R$ scalar bosons and the mass of the heaviest RH neutrino that must be 2 to 10 times smaller for $M_{W_R} = 3.5$ TeV. These bounds are however derived under the assumption that light neutrino mass arises from either a type I or a type II seesaw mechanism. Considering a scenario with a combination of type I and type II seesaw mechanisms (as in this work) enables us to evade those bounds, as also

pointed out earlier by [59, 58]. The $SU(2)_R$ triplet scalar masses are allowed to be even smaller than the heaviest RH neutrino mass. RH neutrinos could nevertheless be indirectly constrained by neutrinoless double-beta decays and cosmology [79, 80, 81].

The constraints from NDBD and CLFV can be complementary to the collider bounds on LRSM, as pointed out by works like [82]. For example, NDBD constraints can rule out some part of the parameter space in the plane of the lightest RH neutrino mass M_N and W_R mass where the LHC limits [77] are weak. As can be seen from the plots of figure 6.20, NDBD constraints can rule out lightest RH neutrino mass as low as 1 GeV, which remains allowed from LHC limits on same sign dilepton searches [77]. This also agrees with the estimates derived in the earlier works mentioned above. In another recent work [83], prospects of probing the $M_N - M_{W_R}$ plane to a much wider extent at several experiments including future colliders and future NDBD experiments were considered. Even in these studies, the collider and NDBD sensitivities were found to be complementary with NDBD experiments putting stronger limits on low $M_N \leq \mathcal{O}(10\text{ GeV})$ while colliders can probe high mass region $M_N \sim \mathcal{O}(\text{TeV})$.

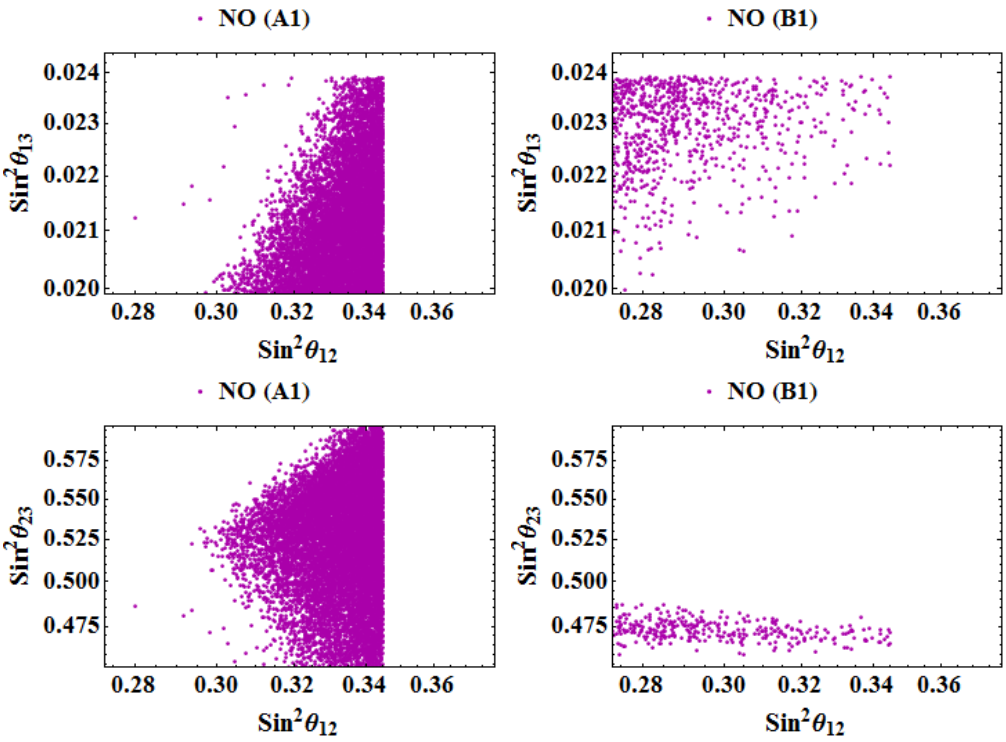

Figure 6.1: Correlation between light neutrino parameters in NO case.

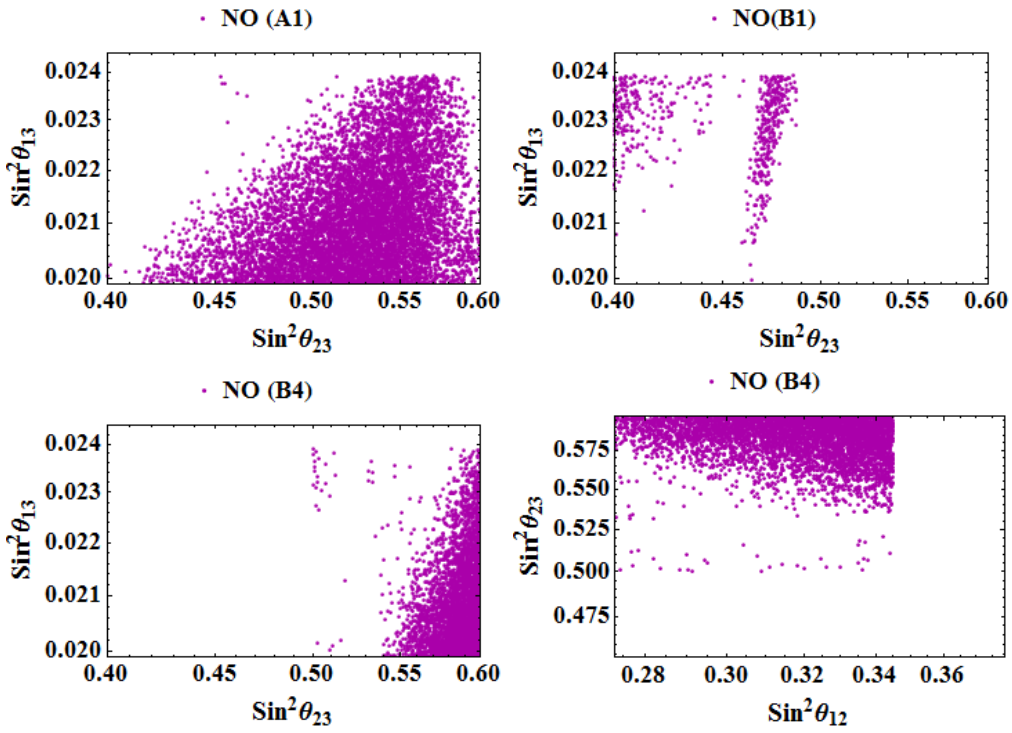

Figure 6.2: Correlation between neutrino parameters in NO case.

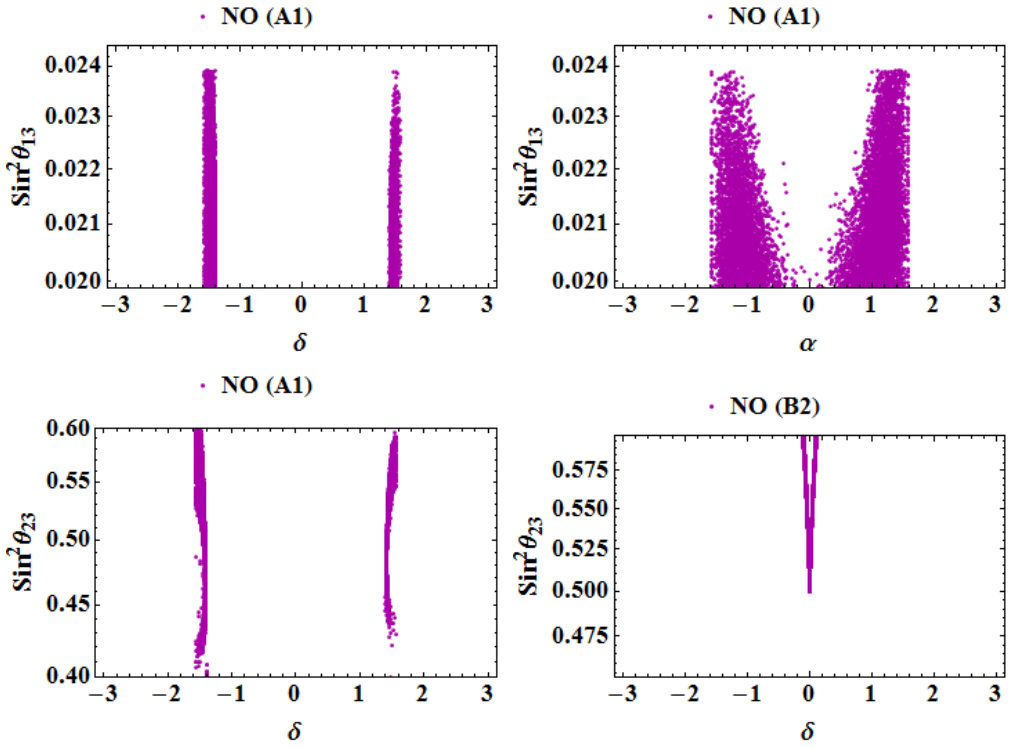

Figure 6.3: Correlation between neutrino parameters in NO case.

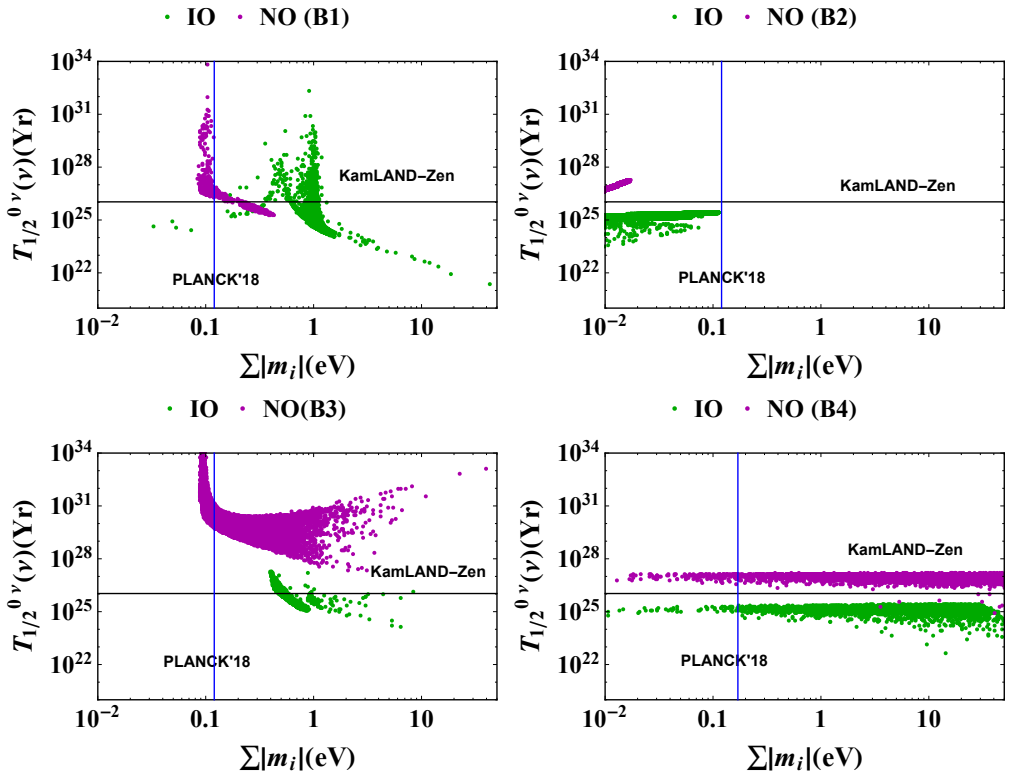

Figure 6.4: Light neutrino contribution to half-life governing NDBD as a function of the sum of light neutrino mass. The solid blue (vertical) and black (horizontal) line represents the Planck upper bound of sum of absolute neutrino mass and the KamLAND-Zen lower limit on half-life respectively.

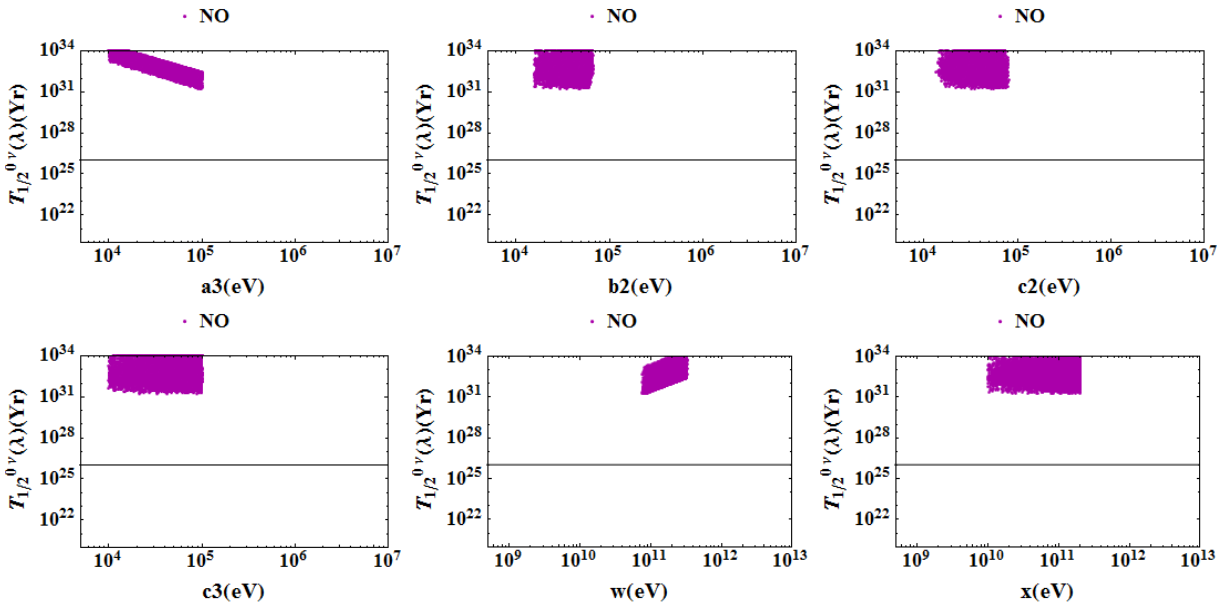

Figure 6.5: λ contribution to half-life governing NDBD as a function of model parameters for the class A1. The horizontal line represents the KamLAND-Zen lower limit.

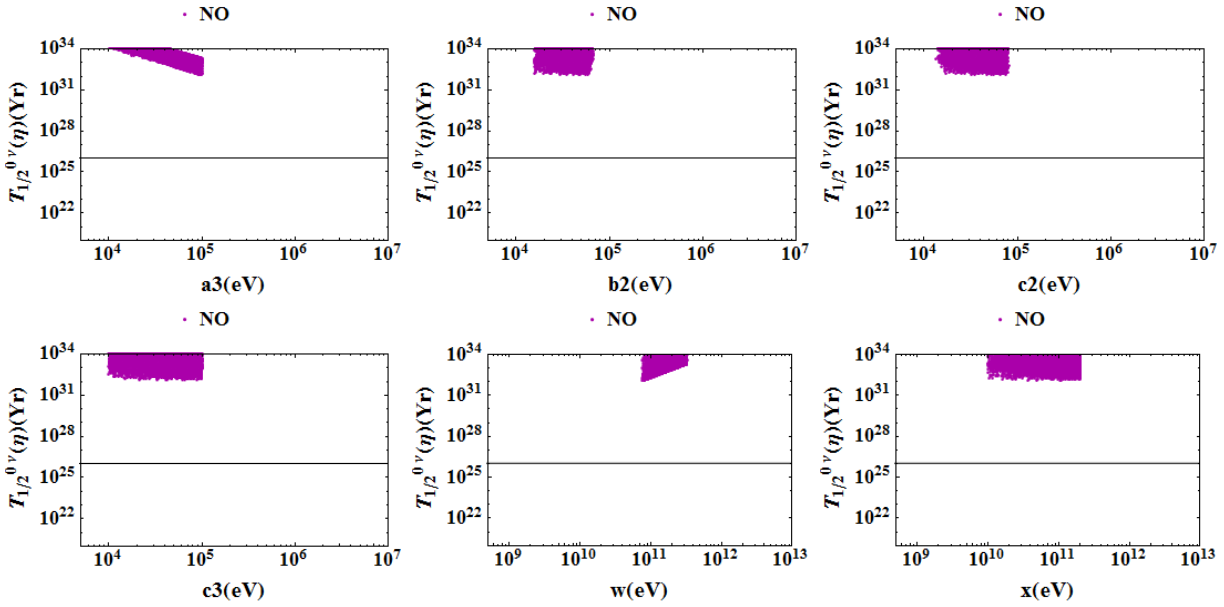

Figure 6.6: η contribution to half-life governing NDBD as a function of model parameters for the class A1. The horizontal line represents the KamLAND-Zen lower limit.

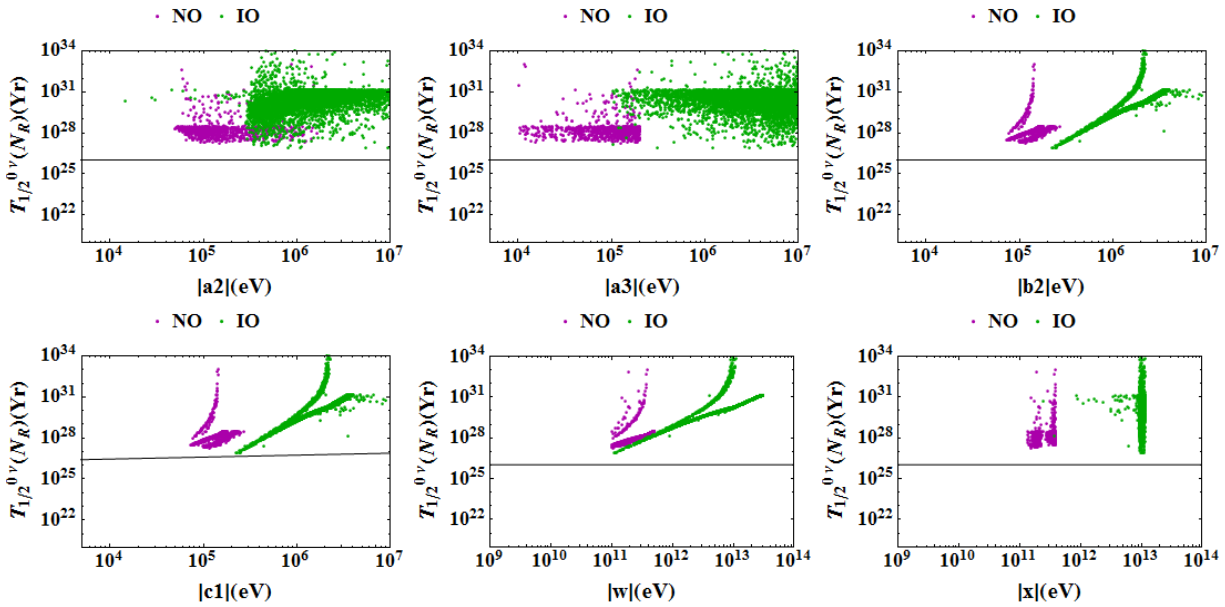

Figure 6.7: Heavy ν (N) contribution to half-life governing NDBD as a function of model parameters for the class B1. The horizontal line represents the KamLAND-Zen lower limit.

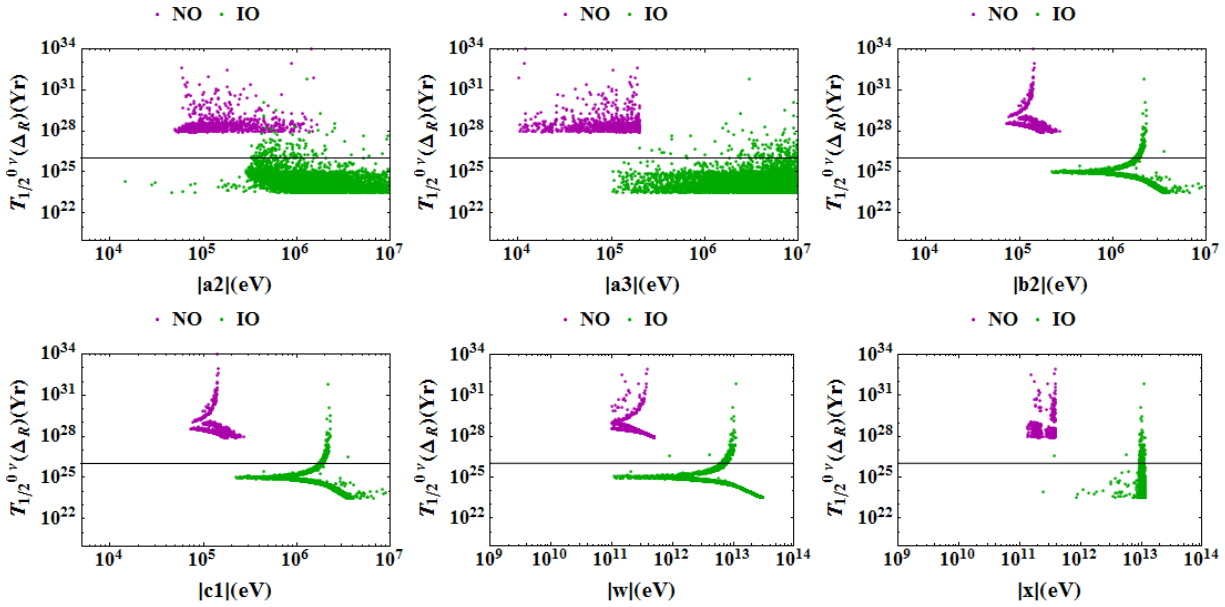

Figure 6.8: Heavy Δ_R contribution to half-life governing NDBD as a function of model parameters for the class B1. The horizontal line represents the KamLAND-Zen lower limit.

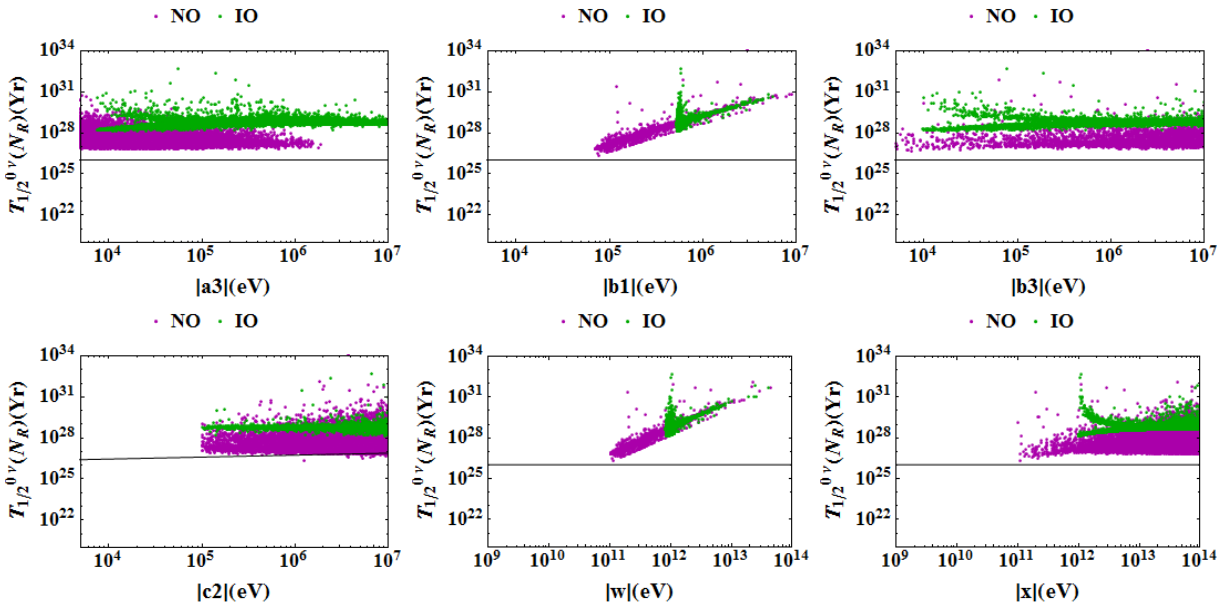

Figure 6.9: Heavy ν (N) contribution to half-life governing NDBD as a function of model parameters for the class B2. The horizontal line represents the KamLAND-Zen lower limit.

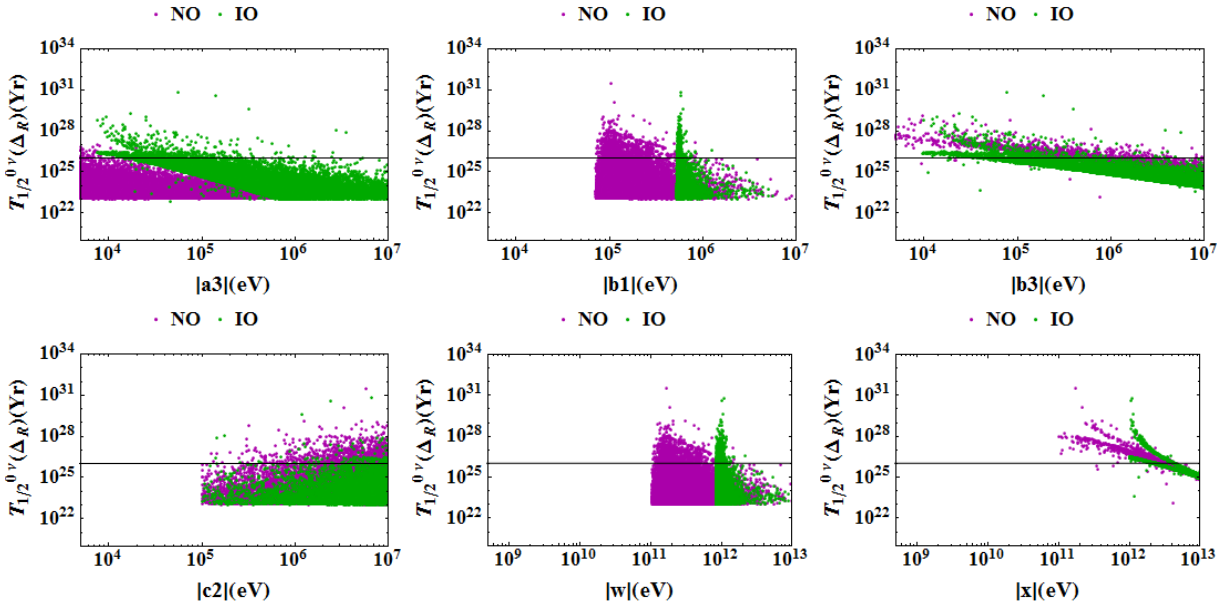

Figure 6.10: Heavy Δ_R contribution to half-life governing NDBD as a function of model parameters for the class B2. The horizontal line represents the KamLAND-Zen lower limit.

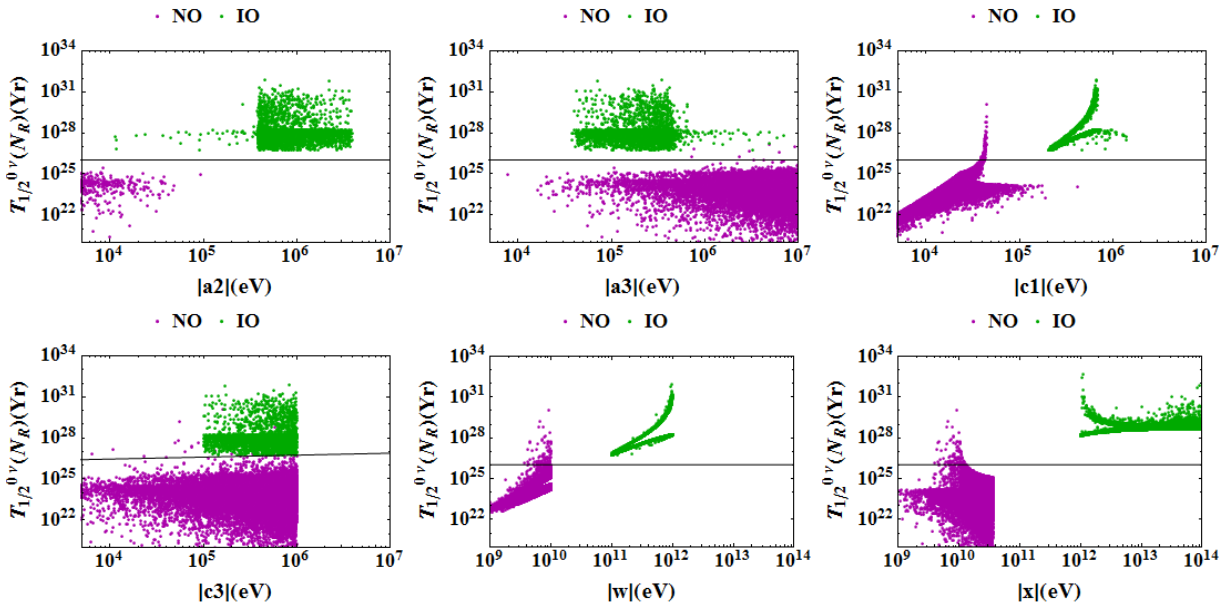

Figure 6.11: Heavy ν (N) contribution to half-life governing NDBD as a function of model parameters for the class B3. The horizontal line represents the KamLAND-Zen lower limit.

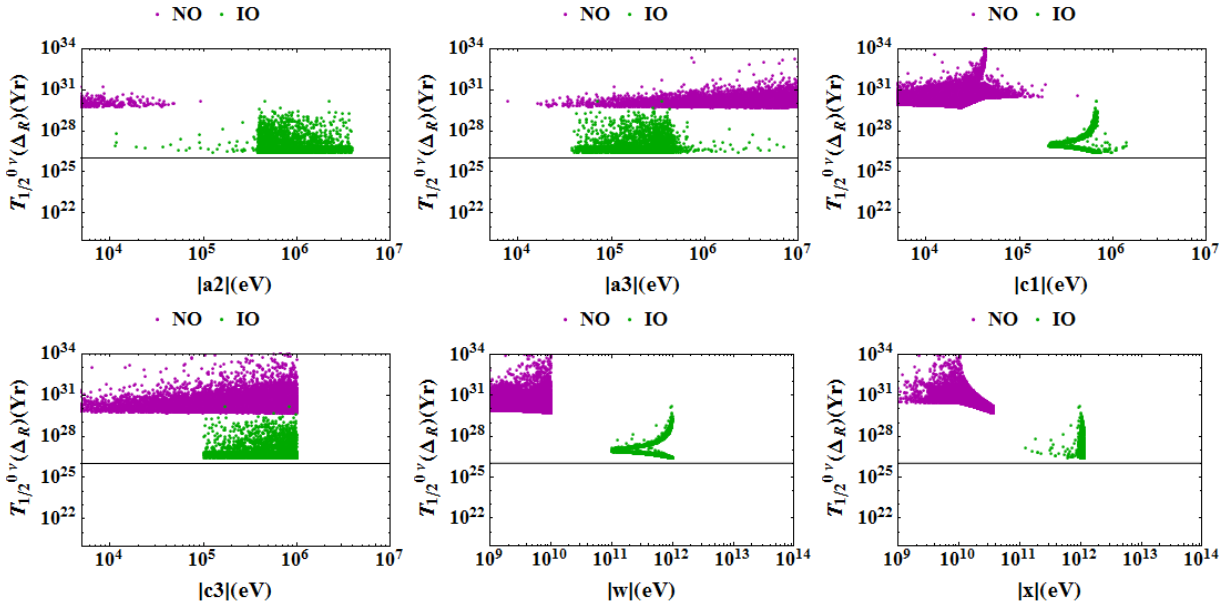

Figure 6.12: Heavy Δ_R contribution to half-life governing NDBD as a function of model parameters for the class B3. The horizontal line represents the KamLAND-Zen lower limit.

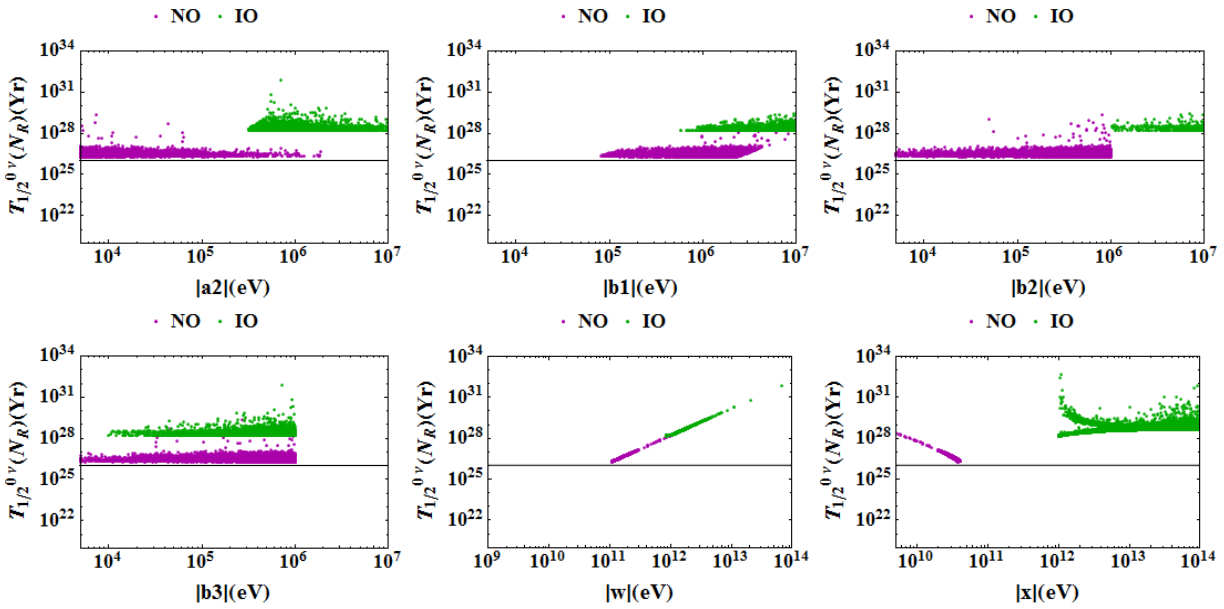

Figure 6.13: Heavy ν (N) contribution to half-life governing NDBD as a function of model parameters for the class B4. The horizontal line represents the KamLAND-Zen lower limit.

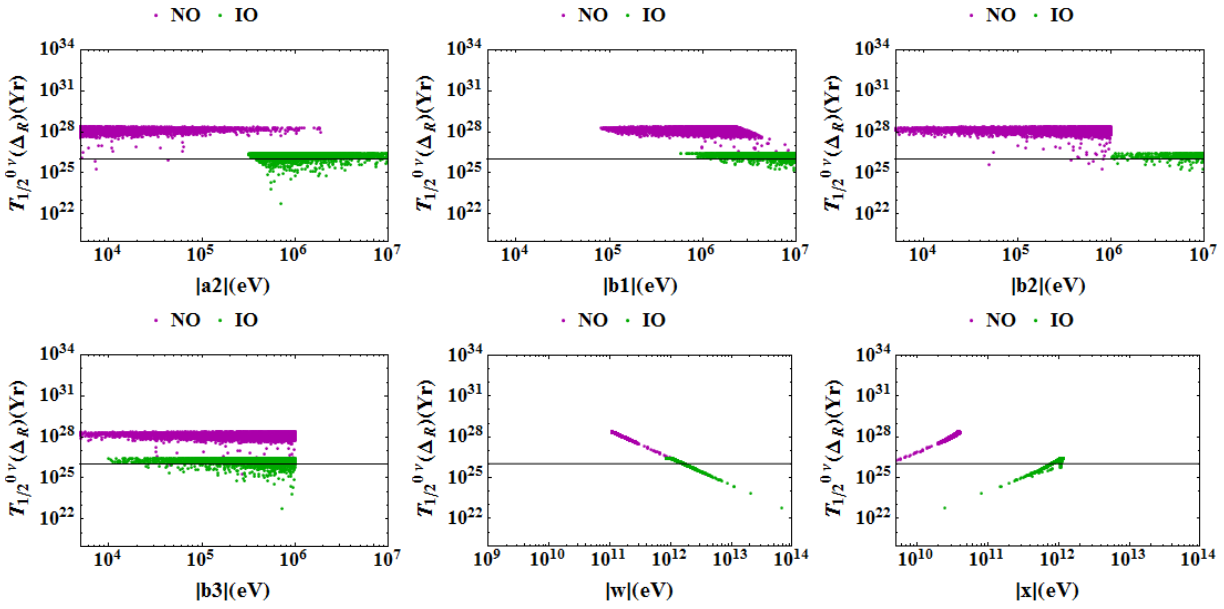

Figure 6.14: Δ_R contribution to half-life governing NDBD as a function of model parameters for the class B4. The horizontal line represents the KamLAND-Zen lower limit.

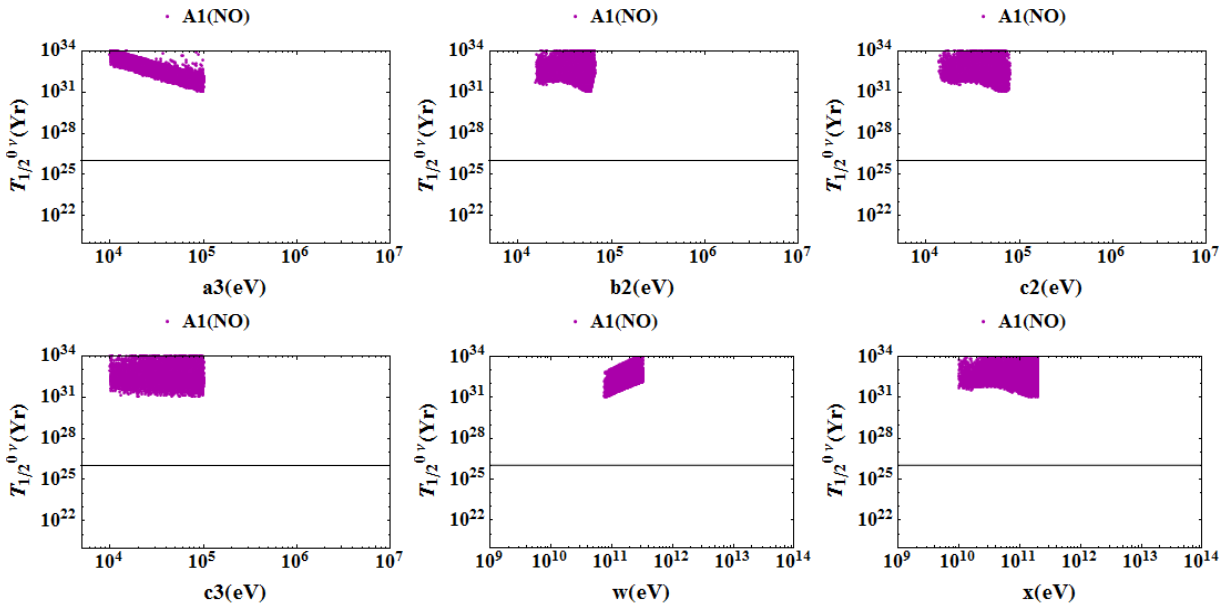

Figure 6.15: Total contribution to half-life governing NDBD as a function of the model parameters for the class A1. The horizontal line represents the KamLAND-Zen lower limit

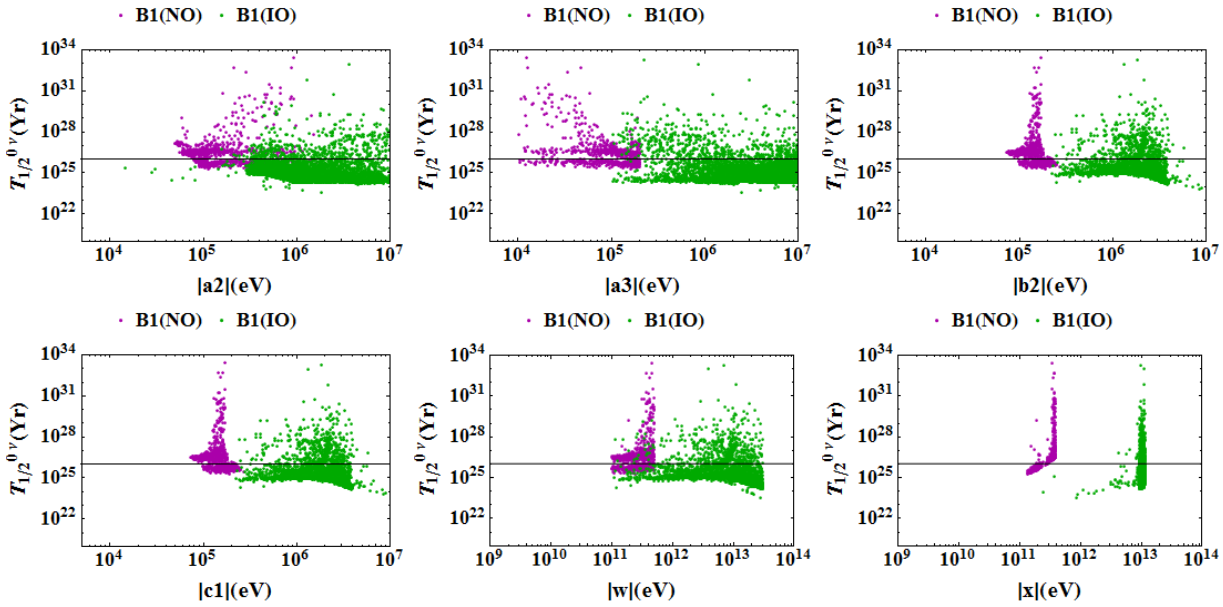

Figure 6.16: Total contribution to half-life governing NDBD as a function of the model parameters for the class B1. The horizontal line represents the KamLAND-Zen lower limit.

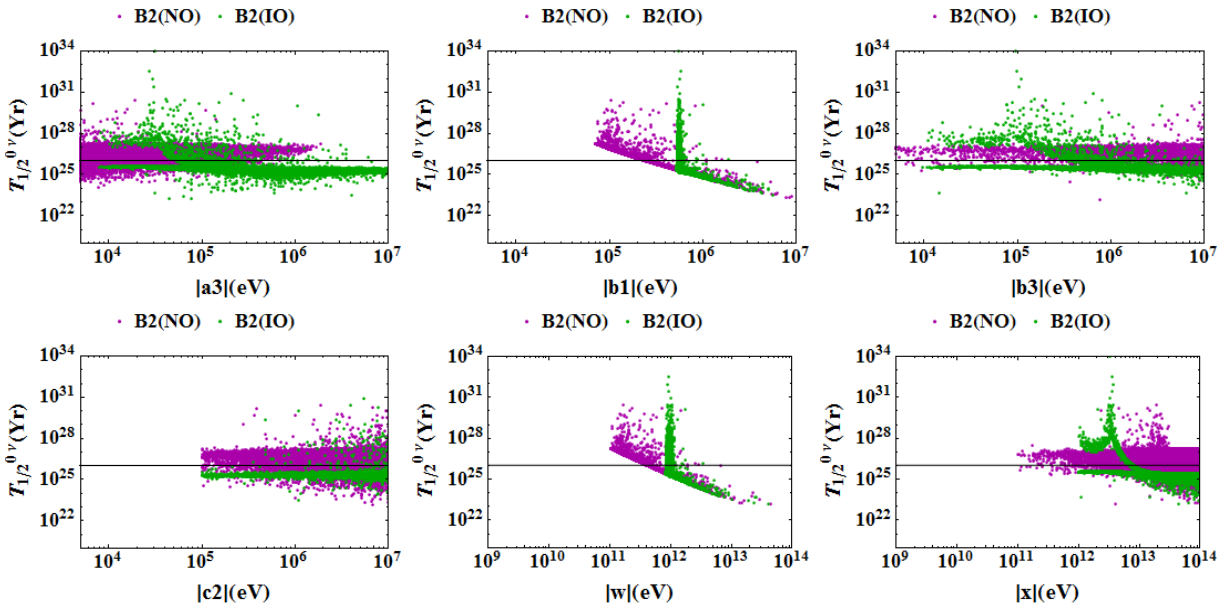

Figure 6.17: Total contribution to half-life governing NDBD as a function of the model parameters for the class B2. The horizontal line represents the KamLAND-Zen lower limit.

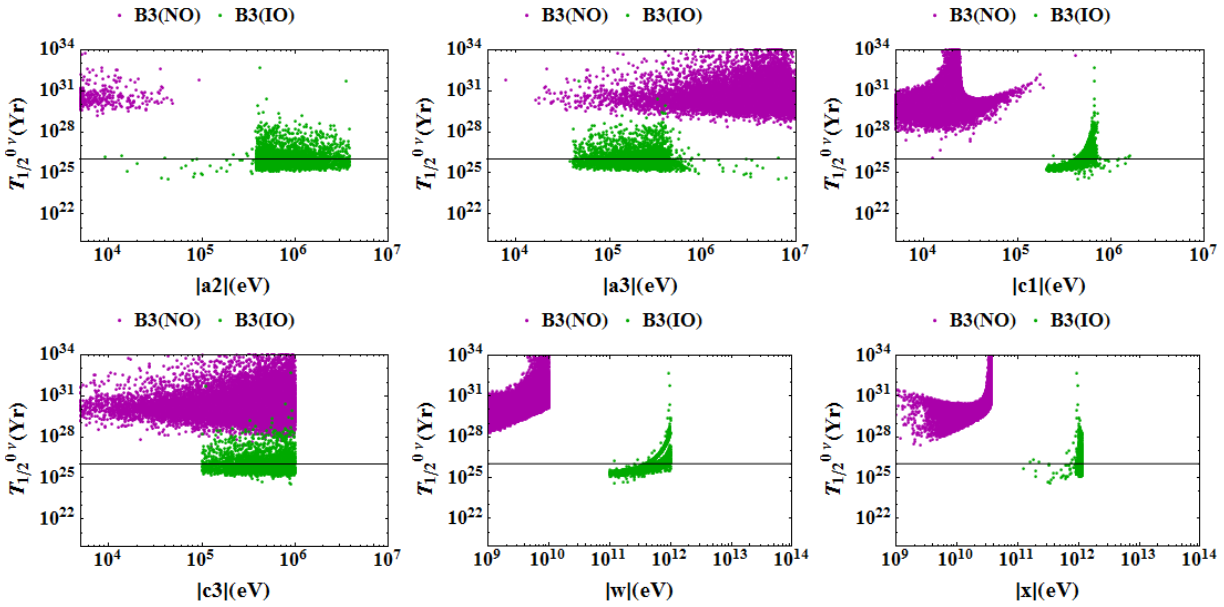

Figure 6.18: Total contribution to half-life governing NDBD as a function of the model parameters for the class B3. The horizontal line represents the KamLAND-Zen lower limit.

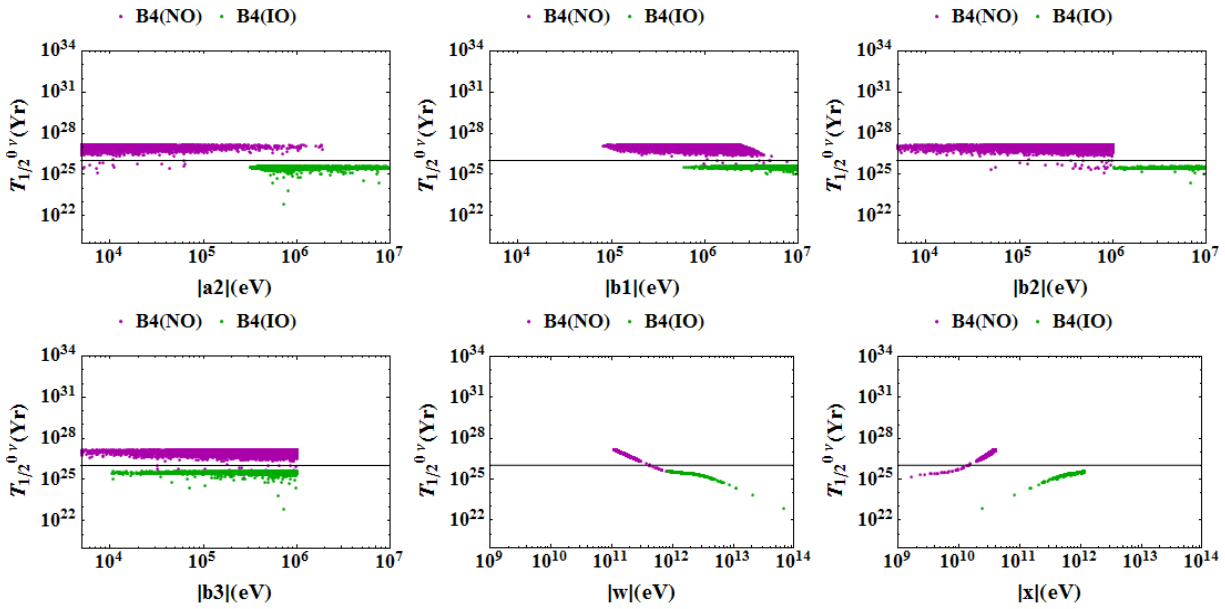

Figure 6.19: Total contribution to half-life governing NDBD as a function of the model parameters for the class B4. The horizontal line represents the KamLAND-Zen lower limit.

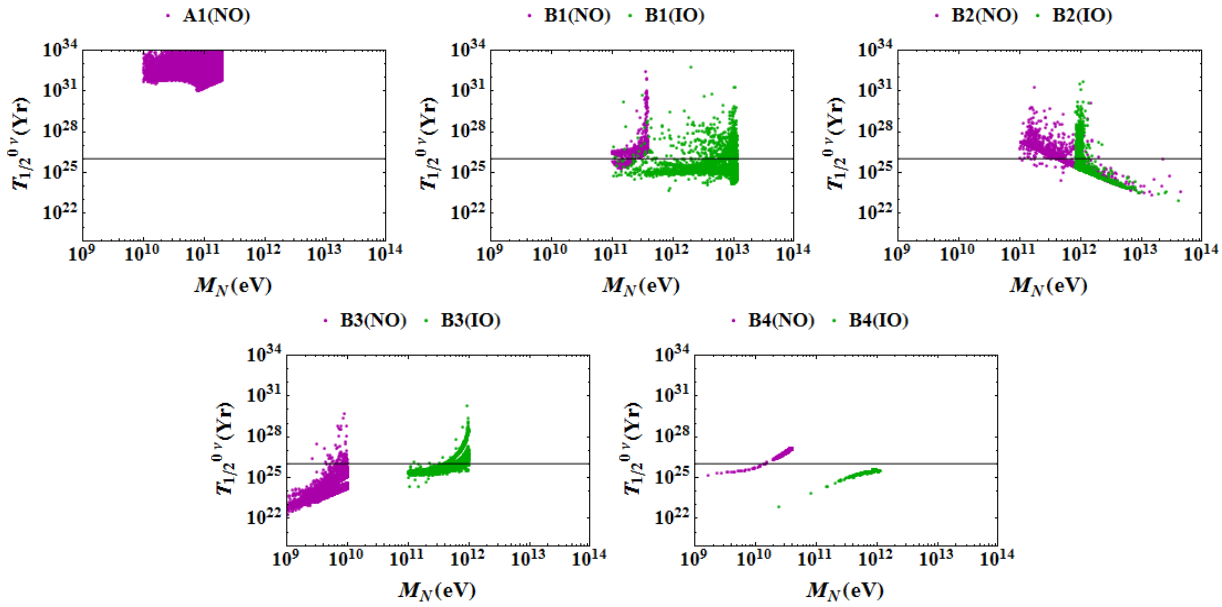

Figure 6.20: Total contribution to half-life governing NDBD as a function of the lightest right handed neutrino mass.

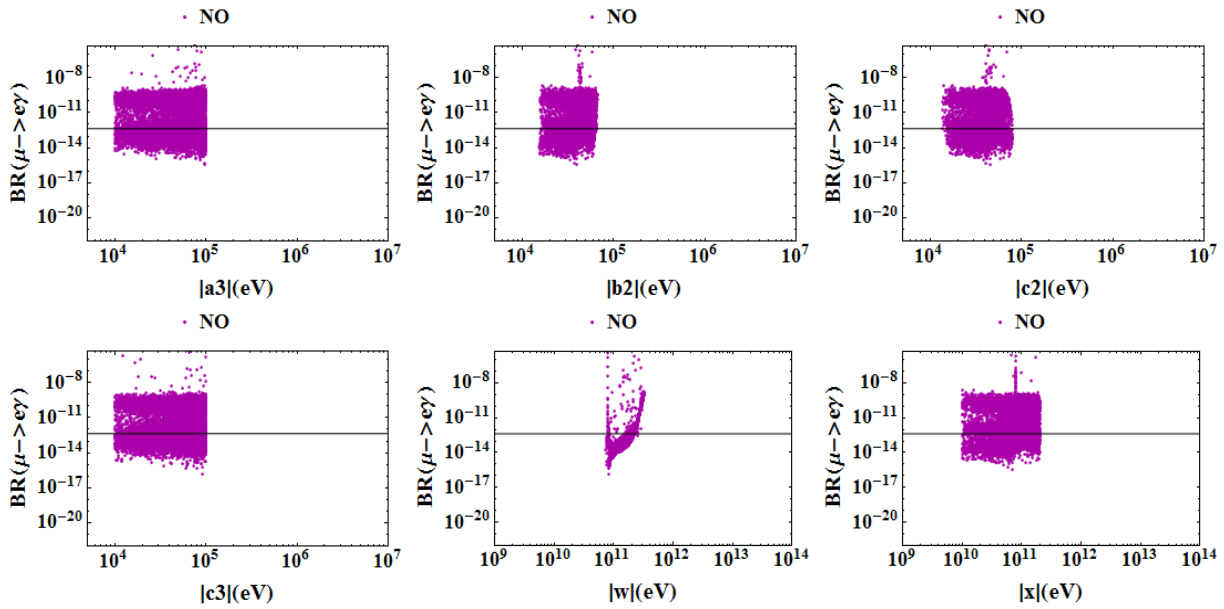

Figure 6.21: BR for $\mu \to e\gamma$ as a function of model parameters for the class A1. The horizontal line represents the upper limit for BR given by MEG experiment.

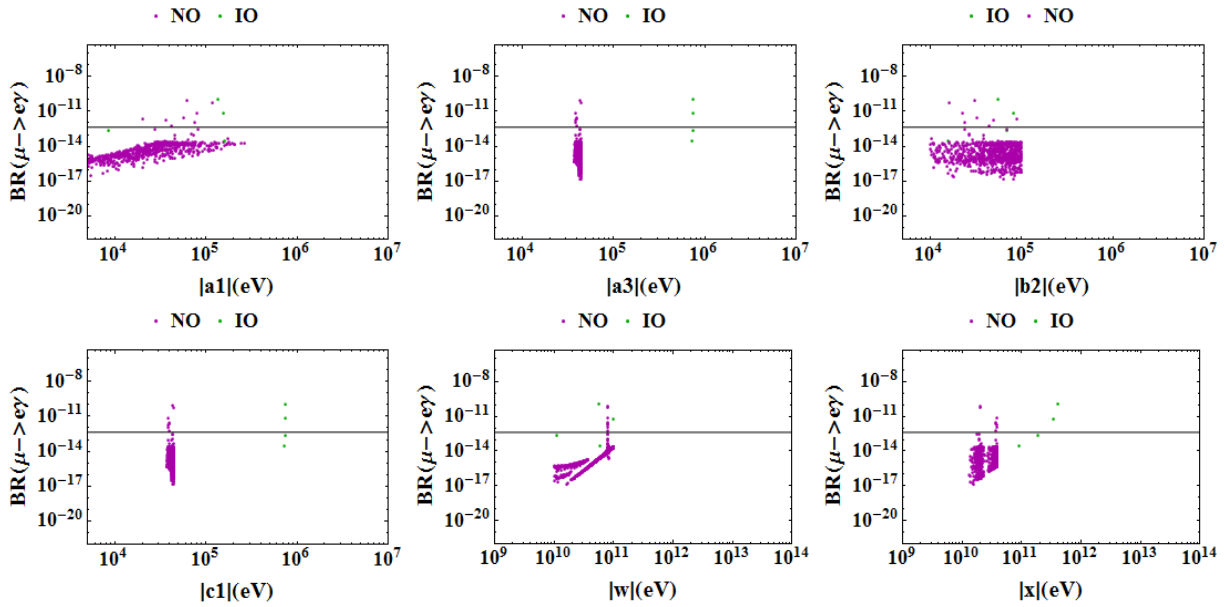

Figure 6.22: BR for $\mu \to e\gamma$ as a function of model parameters for the class B1. The horizontal line represents the upper limit for BR given by MEG experiment.

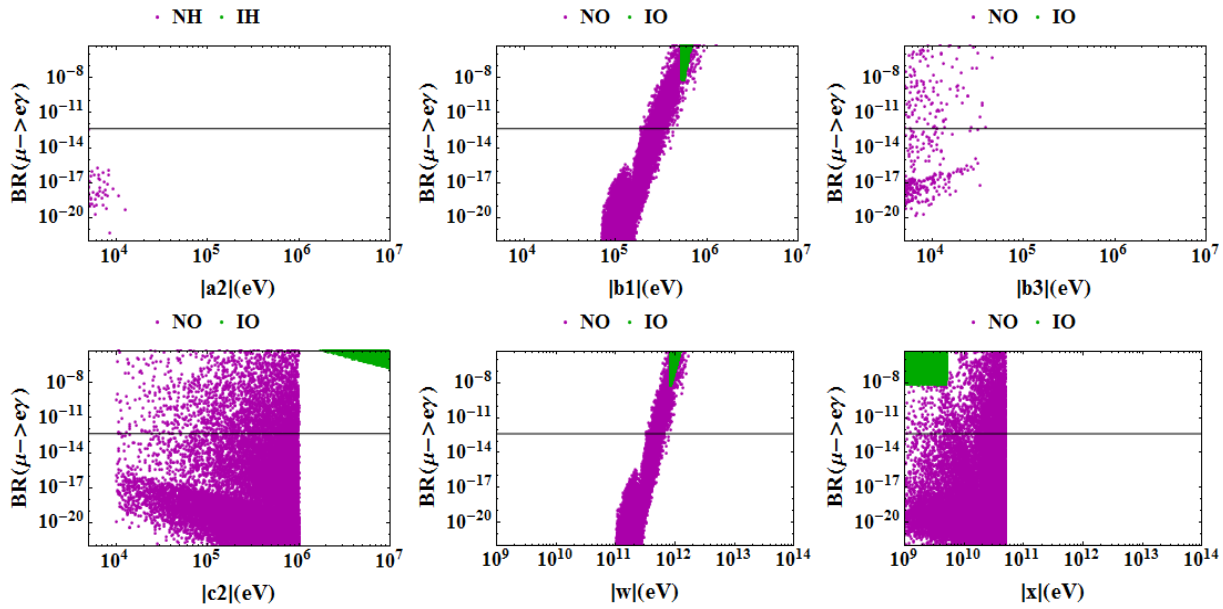

Figure 6.23: BR for $\mu \to e\gamma$ as a function of model parameters for the class B2. The horizontal line represents the upper limit for BR given by MEG experiment.

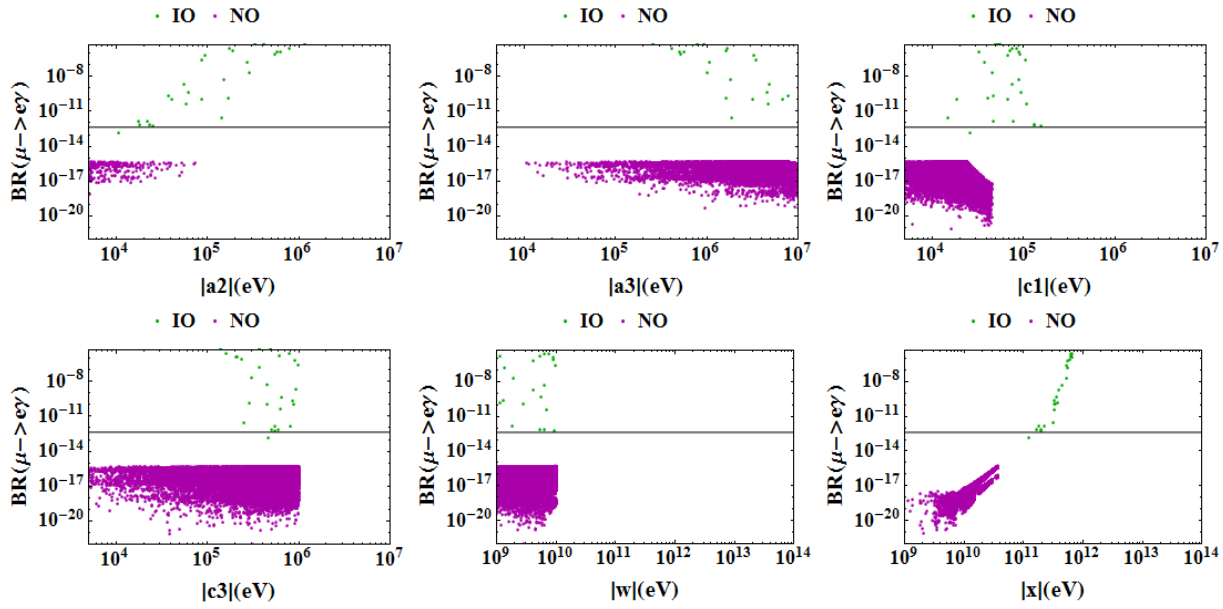

Figure 6.24: BR for $\mu \to e\gamma$ as a function of model parameters for the class B3. The horizontal line represents the upper limit for BR given by MEG experiment.

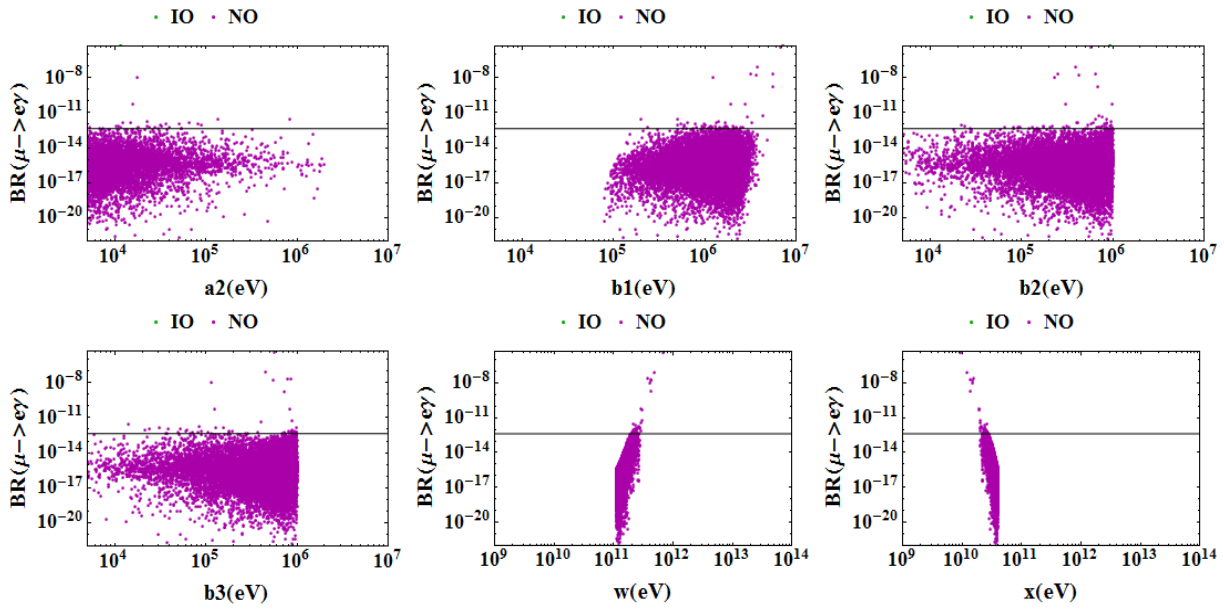

Figure 6.25: BR for $\mu \to e\gamma$ as a function of model parameters for the class B4. The horizontal line represents the upper limit for BR given by MEG experiment.

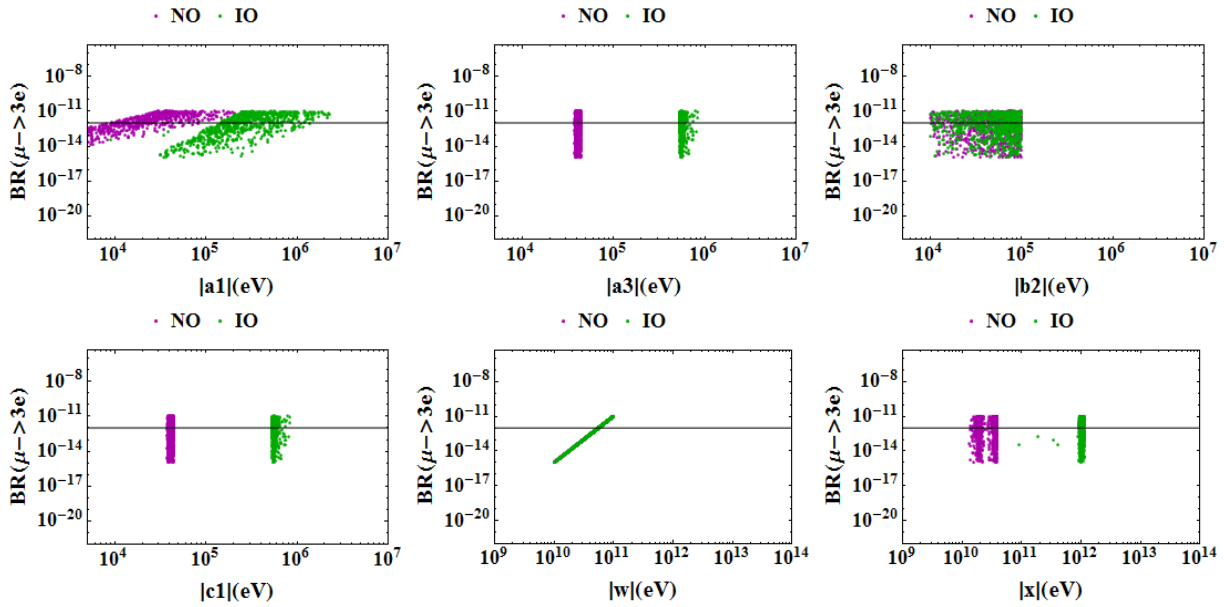

Figure 6.26: BR for $\mu \to 3e$ as a function of model parameters for the class B1. The horizontal line represents the upper limit for BR given by SINDRUM experiment.

Class	NDBD (Total half-life)	BR($\mu \to e\gamma$)	BR($\mu \to 3e$)
A1(NO/IO)	✓(×)	✓(×)	✓(✓)
B1(NO/IO)	✓(✓)	✓(✓)	✓(✓)
B2(NO/IO)	✓(✓)	✓(×)	✓(✓)
B3(NO/IO)	✓(✓)	✓(✓)	✓(✓)
B4(NO/IO)	✓(×)	✓(×)	✓(✓)

Table 6.5: Summary of allowed and disallowed textures. The ✓ and × symbol are used to denote if the observables (NDBD/CLFV) are (not are) within the current experimental upper limit.

Class	ν_L	${N_R}^R$	${N_R}^L$	Δ_R	λ	η	BR($\mu \to e\gamma$)	BR($\mu \to 3e$)
A1							NO	
B1	NO/IO	NO/IO		NO/IO			NO/IO	NO/IO
B2	NO	NO/IO	NO/IO	NO/IO			NO	
B3	NO/IO	IO		NO/IO			NO/IO	
B4	NO	NO/IO		NO/IO			NO	

Table 6.6: Summarized form of the results only for the allowed cases pointing out the individual contributions to NDBD as well as the total CLFV contributions which can saturate corresponding experimental upper limits for both NO and IO. The empty boxes correspond to the contributions which remain subdominant.

6.6 Discussion and Conclusion

We have studied the possibility of texture zeros in lepton mass matrices of the minimal left-right symmetric model where light neutrino mass arises from a combination of type I and type II seesaw mechanism. Considering the allowed texture zeros in light neutrino mass matrix, we list out all possible texture zero possibilities in Dirac and heavy neutrino mass matrices which play a role in type I and type II seesaw mechanism. After making

this exhaustive list in table 6.1, we consider, for our numerical studies, the possibility with a maximum allowed zeros in M_ν, M_D and M_{RR} while keeping the rank of the latter three. After finding the allowed parameter space for two zero textures in light neutrino mass matrix M_ν, we then evaluate the elements of M_D, M_{RR} by choosing an optimistic $M_{W_R} = 4.5$ TeV while keeping the RH neutrino masses above 1 GeV. We then evaluate the contributions to NDBD half-life as well as CLFV decays $\mu \to e\gamma, \mu \to 3e$ and constrain the texture zero mass matrices from the relevant experimental bounds. The summary of our results is shown in table 6.5. It is seen that out of all the cases considered with 5-0 M_D and $4-0$ M_{RR}, only A1 (NO), B1 (NO/IO), B2 (NO), B3 (NO/IO), B4 (NO) are allowed from both NDBD and CLFV constraints while the others are disallowed by at least one of the constraints. In table 6.6, we further show the allowed cases pointing out the individual contributions to NDBD and total contributions to CLFV which can saturate the current experimental upper bound, keeping them sensitive to ongoing and future experiments. It is interesting to note that even for the most conservative lower bound on left-right symmetry scale that is $M_{W_R} = 4.5$ TeV from collider experiment, the complementary bounds from rare decay experiments can rule out several texture possibilities while keeping the allowed ones sensitive to upcoming experiments. We performed our study from a phenomenological point of view keeping the framework as minimal as the minimal LRSM. We leave a more detailed study of these interesting texture zero scenarios within additional flavor symmetry for future works.

Bibliography

[1] Planck collaboration, Aghanim, N., et al. Planck 2018 results. VI. Cosmological parameters, *arXiv:1807.06209*, 2018.

[2] Pati, J. C. and Salam, A. Lepton Number as the Fourth Color. *Phys. Rev. D*, 10:275, 1974.

[3] Mohapatra, R. N. and Pati, J. C. Left-Right Gauge Symmetry and an Isoconjugate Model of CP Violation. *Phys. Rev. D*, 11: 566, 1975.

[4] Mohapatra, R. and Pati, J. C. A Natural Left-Right Symmetry. *Phys. Rev. D*, 11;2258, 1975.

[5] Senjanovic, G. and Mohapatra R. N. Exact Left-Right Symmetry and Spontaneous Violation of Parity. *Phys. Rev. D*, 12:1502, 1975.

[6] Mohapatra, R. N., Paige, F. E. and Sidhu, D. P. Symmetry Breaking and Naturalness of Parity Conservation in Weak Neutral Currents in Left-Right Symmetric Gauge Theories. *Phys. Rev. D*, 17:2462, 1978.

[7] Senjanovic, G. Spontaneous Breakdown of Parity in a Class of Gauge Theories. *Nucl. Phys. B*, 153:334, 1979.

[8] Mohapatra, R. N. and Marshak, R. E. Local B- L symmetry of electroweak interactions, majorana neutrinos, and neutron oscillations. *Phys. Rev. Lett.*, 44 (20): 1316, 1980.

[9] Lim, C. S. and Inami, T. Lepton Flavor Nonconservation and the MassGeneration Mechanism for Neutrinos. *Prog. Theor. Phys.*, 67:1569, 1982.

[10] Gunion, J. F., Grifols, J., Mendez, A., Kayser, B. and Olness, F. I. Higgs Bosons in Left-Right Symmetric Models. *Phys. Rev. D*, 40: 1546, 1989.

[11] Deshpande, N. G., Gunion, J. F, Kayser, B. and Olness, F. I. Left-right symmetric electroweak models with triplet Higgs. *Phys. Rev. D*, 44: 837, 1991.

[12] Fileviez Perez, P. Type III Seesaw and Left-Right Symmetry. *JHEP*, 03:142, 2009.

[13] Ioannisian, A. and Valle, J. W. F. SO(10) grand unification model for degenerate neutrino masses. *Phys. Lett. B*, 332: 93-99, 1994.

[14] Bamert, P. and Burgess, C. P. Naturally degenerate neutrinos. *Phys. Lett. B*, 329:289-294, 1994.

[15] Antusch, S. F., Steve F. From hierarchical to partially degenerate neutrinos via type II upgrade of type I seesaw models. *Nucl. Phys. B*, 705:239-268, 2005.

[16] Aaboud, M., et al. Search for a new heavy gauge boson resonance decaying into a lepton and missing transverse momentum in 36 fb^{-1} of pp collisions at $\sqrt{s} = 13$ TeV with the ATLAS experiment. *arXiv:1706.04786*, 2017.

[17] Aaboud, M., et al. Search for new phenomena in dijet events using 37 fb^{-1} of pp collision data collected at $\sqrt{s}$ =13 TeV with the ATLAS detector. *Phys. Rev. D*, 96(5):052004, 2017.

[18] Sirunyan, A. M. et al. Search for high-mass resonances in final states with a lepton and missing transverse momentum at $\sqrt{s} = 13$ TeV. *arXiv:1803.11133*, 2018.

[19] Ludl, P. O. and Grimus, W. A complete survey of texture zeros in the lepton mass matrices. *JHEP*, 07:090, 2014.

[20] Xing, Z.-z. Texture zeros and Majorana phases of the neutrino mass matrix. *Phys. Lett. B*, 530: 159, 2002.

[21] Singh, M., Ahuja, G. and Gupta, M. Revisiting the texture zero neutrino mass matrices. *PTEP* 2016:123B08, 2016.

[22] Ahuja, G. Texture Zero Mass Matrices and Their Implications. *Bled Workshops Phys.*, 18:1, 2017.

[23] Borah, M., Borah, D. and Das, M. K. Discriminating Majorana neutrino textures in light of the baryon asymmetry. *Phys. Rev. D*, 91:113008, 2015.

[24] Kalita, R. and Borah, D. Hybrid Textures of Neutrino Mass Matrix under the Lamp-post of Latest Neutrino and Cosmology Data. *Int. J. Mod. Phys. A*, 31:1650008, 2016.

[25] Meloni, D., Meroni, A. and Peinado, E. Two-zero Majorana textures in the light of the Planck results. *Phys. Rev. D*, 89:053009, 2014.

[26] Fritzsch, H., Xing, Z. Z. and Zhou, S. Two-zero Textures of the Majorana Neutrino Mass Matrix and Current Experimental Tests. *JHEP*, 09:083, 2011.

[27] Alcaide, J., Salvado, J. and Santamaria, A. Fitting flavour symmetries: the case of two-zero neutrino mass textures. *JHEP*, 07:164, 2018.

[28] Zhou, S. Update on two-zero textures of the Majorana neutrino mass matrix in light of recent T2K, Super-Kamiokande and NOνA results. *Chin. Phys. C*, 40:033102, 2016.

[29] Bora, K., Borah, D. and Dutta, D. Probing Majorana Neutrino Textures at DUNE. *Phys. Rev. D*, 96:075006, 2017.

[30] Borah, D., Ghosh, M., Gupta, S. Prakash, S. and Raut, S. K. Analysis of four-zero textures in the $3 + 1$ neutrino framework. *Phys. Rev. D*, 94(11):113001, 2016.

[31] Borah, D., Ghosh, M., Gupta, S. and Raut, S. K. Texture zeros of low-energy Majorana neutrino mass matrix in 3+1 scheme. *Phys. Rev. D*, 96(5):055017, 2017.

[32] Sarma, N., Bora, K. and Borah, D. Compatibility of A_4 Flavour Symmetric Minimal Extended Seesaw with $(3 + 1)$ Neutrino Data. *Eur. Phys. J. C*, 79(2):129, 2019.

[33] Nath, N., Ghosh, M., Goswami, S. and Gupta, S. Phenomenological study of extended seesaw model for light sterile neutrino. *JHEP*, 03:075, 2017.

[34] Gu, P. H., and Hirsch, M., Sarkar, U. and Valle, J. W. F. Neutrino masses, leptogenesis and dark matter in hybrid seesaw. *Phys. Rev. D*, 79:033010, 2009.

[35] Deppisch, F. F. Lepton Flavour Violation and Flavour Symmetries. *Fortsch. Phys.*, 61:622-644, 2013.

[36] Carcamo Hernandez, A. E. and Kovalenko, S., Valle, J. W. F. and Vaquera-Araujo, C. A. Neutrino predictions from a left-right symmetric flavored extension of the standard model. *JHEP*, 02:065, 2019.

[37] Lamprea, J. M. and Peinado, E. Seesaw scale discrete dark matter and two-zero texture Majorana neutrino mass matrices. *Phys. Rev. D*, 94(5):055007, 2016.

[38] De La V, L. M. G. and Ferro-Hernandez, R. and Peinado, E. Simple A_4 models for dark matter stability with texture zeros. *Phys. Rev. D*, 99(5):055044, 2019.

[39] Cebola, L. M., Emmanuel-Costa, D.,and Felipe, R. G. Confronting predictive texture zeros in lepton mass matrices with current data. *Phys. Rev. D*, 92(2):025005, 2015.

[40] Berger, M. S. and Siyeon, K. Discrete flavor symmetries and mass matrix textures. *Phys. Rev. D*, 64:053006, 2001.

[41] Grimus, W. and Joshipura, A. S. Lavoura, L. and Tanimoto, M. Symmetry realization of texture zeros. *Eur. Phys. J. C*, 36:227-232, 2004.

[42] Dev, S., Gupta, S. and Gautam, R. R. Zero Textures of the Neutrino Mass Matrix from Cyclic Family Symmetry. *Phys. Lett. B*, 701:605-608, 2011.

[43] Rodejohann, W. Neutrino-less Double Beta Decay and Particle Physics. *Int. J. Mod. Phys.*, E20:1833-1930, 2011.

[44] Cardani, L. Neutrinoless Double Beta Decay Overview. *arXiv: 1810.12828*, 2018.

[45] Dolinski, M. J. and Poon, A. W. P. and Rodejohann, W. Neutrinoless Double-Beta Decay: Status and Prospects. *arXiv: 1902.04097*, 2019.

[46] Mohapatra, R. N. New Contributions to Neutrinoless Double beta Decay in Supersymmetric Theories. *Phys. Rev. D*, 34:3457-3461, 1986.

[47] Babu, K. S. and Mohapatra, R. N. New vector-scalar contributions to neutrinoless double beta decay and constraints on R-parity violation. *Phys. Rev. Lett.*, 75:2276-2279, 1995.

[48] Hirsch, M., Klapdor-Kleingrothaus, H. V. and Kovalenko, S. G. New leptoquark mechanism of neutrinoless double beta decay. *Phys. Rev. D*, 54:4207-4210, 1996.

[49] Deppisch, F. F., Hirsch, M. and Pas, H. Neutrinoless Double Beta Decay and Physics Beyond the Standard Model. *J. Phys. G*, 39:124007, 2012.

[50] Schechter, J. and Valle, J. W. F. Neutrinoless Double beta Decay in SU(2) x U(1) Theories. *Phys. Rev. D*, 25:2951, 1982.

[51] Ge, S. F., and Lindner, M. and Patra, S. New physics effects on neutrinoless double beta decay from right-handed current. *JHEP*, 10:077, 2015.

[52] Awasthi, R. L., Parida, M.K. and Patra, S. Neutrino masses, dominant neutrinoless double beta decay, and observable lepton flavor violation in left-right models and SO(10) grand unification with lowmass W_R, Z_R bosons. *JHEP*, 08:122, 2013.

[53] Patra, S. Neutrinoless double beta decay process in left-right symmetric models without scalar bidoublet. *Phys. Rev. D*, 87(1):015002, 2013.

[54] Chakrabortty, J., Devi, H. Z., Goswami, S. and Patra, S. Neutrinoless double-β decay in TeV scale Left-Right symmetric models. *JHEP*, 08:008, 2012.

[55] Tello, V., Nemevsek, M., Nesti, F., Senjanovic, G. and Vissani, F. Left-Right Symmetry: from LHC to Neutrinoless Double Beta Decay. *Phys. Rev. Lett.*, 106:151801, 2011.

[56] Awasthi, R. L. and Dev, P. S. B. and Mitra, M. Implications of the Diboson Excess for Neutrinoless Double Beta Decay and Lepton Flavor Violation in TeV Scale Left Right Symmetric Model. *Phys. Rev. D*, 93(1):011701, 2016.

[57] Huang, W. C. and Lopez-Pavon, J. On neutrinoless double beta decay in the minimal left-right symmetric model. *Eur. Phys. J. C*, 74:2853, 2014.

[58] Borah, D. and Dasgupta, A. Charged lepton flavour violation and neutrinoless double beta decay in left-right symmetric models with type I+II seesaw. *JHEP*, 07:022, 2016.

[59] Borah, D. and Dasgupta, A. Neutrinoless Double Beta Decay in Type I+II Seesaw Models. *JHEP*, 11:208, 2015.

[60] Hirsch, M. and Klapdor-Kleingrothaus, H. V. and Panella, O. Double beta decay in left-right symmetric models. *Phys. Lett. B*, 374:7-12, 1996.

[61] Bambhaniya, G., Dev, P. S. B. and Goswami, S. and Mitra, M. The Scalar Triplet Contribution to Lepton Flavour Violation and Neutrinoless Double Beta Decay in Left-Right Symmetric Model. *JHEP*, 04:046, 2016.

[62] Dev, P. S. B.,Goswami, S. and Mitra, M. TeV Scale Left-Right Symmetry and Large Mixing Effects in Neutrinoless Double Beta Decay. *Phys. Rev. D*, 91(11):113004, 2015.

[63] Barry, J. and Rodejohann, W. Lepton number and flavour violation in TeV-scale left-right symmetric theories with large left-right mixing. *JHEP*, 09:153, 2013.

[64] Gando, A., et al. Search for Majorana Neutrinos near the Inverted Mass Hierarchy Region with KamLAND-Zen. *Phys. Rev. Lett.*, 117(8):082503, 2016.

[65] Lindner, M., Platscher, M. and Queiroz, F. S. A Call for New Physics : The Muon Anomalous Magnetic Moment and Lepton Flavor Violation. *Phys. Rept.*, 731:1-82, 2018.

[66] Leontaris, G. K., Tamvakis, K. and Vergados, J. D. Lepton and Family Number Violation From Exotic Scalars. *Phys. Lett. B*, 162:153-159, 1985.

[67] Swartz, Morris L. Limits on Doubly Charged Higgs Bosons and Lepton Flavor Violation. *Phys. Rev. D*, 40:1521, 1989.

[68] Cirigliano, V., Kurylov, A., Ramsey-Musolf, M. J. and Vogel, P. Lepton flavor violation without supersymmetry. *Phys. Rev. D*, 70:075007, 2004.

[69] Cirigliano, V., Kurylov, A., Ramsey-Musolf, M. J. and Vogel, P. Neutrinoless double beta decay and lepton flavor violation. *Phys. Rev. Lett.*, 93:231802, 2004.

[70] Bajc, B., and Nemevsek, M. and Senjanovic, G. Probing leptonic CP phases in LFV processes. *Phys. Lett. B*, 684:231-235, 2010.

[71] Bernstein, R. H. and Cooper, P. S. Charged Lepton Flavor Violation: An Experimenter's Guide. *Phys. Rept.*, 532:27-64, 2013.

[72] Fileviez Perez, P. and Murgui, C. Lepton Flavour Violation in Left-Right Theory. *Phys. Rev. D*, 95 (7):075010, 2017.

[73] Baldini, A. M., et al.MEG Upgrade Proposal. *arXiv:1310.7225*, 2013.

[74] Bellgardt, U., et al. Search for the Decay mu+ —> e+ e+ e-. *Nucl. Phys. B*, 299:1-6, 1988.

[75] Esteban, I., Gonzalez-Garcia, M.C., Cabezudo, A.H., Maltoni, M. and Schwetz, T. Global analysis of three-flavour neutrino oscillations: synergies and tensions in the determination of θ_{23}, δ_{CP}, and the mass ordering. *JHEP*, 01:106, 2019.

[76] Borah, D., Dasgupta, A. and Patra, S. Dominant light-heavy neutrino mixing contribution to $0\nu\beta\beta$ in minimal left-right symmetric model with universal seesaw. *Int. J. Mod. Phys. A*, 33:1850198, 2018.

[77] Sirunyan, A. M., et al. Search for a heavy right-handed W boson and a heavy neutrino in events with two same-flavor leptons and twojets at $\sqrt{s} = 13$ TeV., *arXiv:1803.11116*, 2018.

[78] Aaboud, M., et al. Search for doubly charged Higgs boson production in multi-lepton final states with the ATLAS detector using proton-proton collisions at $\sqrt{s} = 13\,\text{TeV}$. *EPJC*, 78:199, 2018.

[79] Borah, D. Light sterile neutrino and dark matter in left-right symmetric models without a Higgs bidoublet. *Phys. Rev. D*, 94(7):075024, 2016.

[80] Frank, M., Fuks, B. Huitu, K., Rai, S. K. and Waltari, H. Resonant slepton production and right sneutrino dark matter in left-right supersymmetry. *JHEP*, 05:015, 2017.

[81] Araz, J. Y., Frank, M. and Fuks, B. Differentiating $U(1)'$ supersymmetric models with right sneutrino and neutralino dark matter. *Phys. Rev. D*, 96(1):015017, 2017.

[82] Das, S. P., Deppisch, F. F., Kittel, O. and Valle, J. W. F. Heavy Neutrinos and Lepton Flavour Violation in Left-Right Symmetric Models at the LHC. *Phys. Rev. D*, 86:055006, 2012.

[83] Lindner, M. and Queiroz, F. S. Rodejohann, W. and Yaguna, Carlos E. Left-Right Symmetry and Lepton Number Violation at the Large Hadron Electron Collider. *JHEP*, 06:140, 2016.